iScience

CellPress

Article

Integrated Regulation of HuR by Translation Repression and Protein Degradation Determines Pulsatile Expression of p53 Under DNA Damage

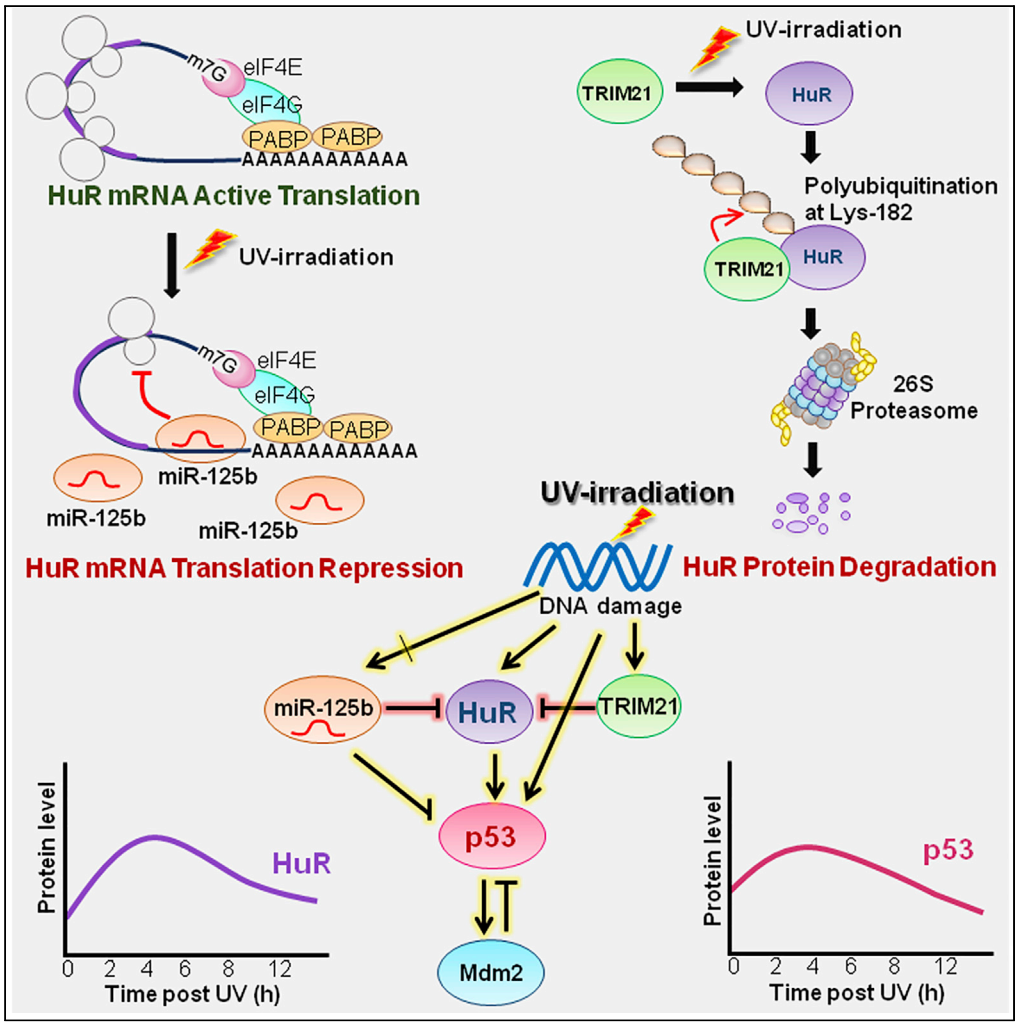

Abhishek Guha, Deepika Ahuja, Sukhen Das Mandal, ..., Belinda Willard, Anandamohan Ghosh, Partho Sarothi Ray

psray@iiserkol.ac.in

HIGHLIGHTS

Systems modeling with experimental validation of p53 translation regulatory network

Includes miR-125b and HuR in the network as upstream regulators of p53 expression

Discovers miR-125b and the E3 ligase TRIM21 as new regulators of HuR in the network

miR-125b and TRIM21 affect cell viability via p53 in response to UV-induced DNA damage

Guha et al., iScience *15*, 342–359
May 31, 2019
https://doi.org/10.1016/j.isci.2019.05.002

iScience

CellPress

Article

Integrated Regulation of HuR by Translation Repression and Protein Degradation Determines Pulsatile Expression of p53 Under DNA Damage

Abhishek Guha,[1,10] Deepika Ahuja,[1,10] Sukhen Das Mandal,[1,11] Bibudha Parasar,[2,6,11] Krishanu Deyasi,[3,7] Debadrita Roy,[1,8] Vasundhara Sharma,[1,9] Belinda Willard,[4] Anandamohan Ghosh,[5] and Partho Sarothi Ray[1,12,*]

SUMMARY

Expression of tumor suppressor p53 is regulated at multiple levels, disruption of which often leads to cancer. We have adopted an approach combining computational systems modeling with experimental validation to elucidate the translation regulatory network that controls p53 expression post DNA damage. The RNA-binding protein HuR activates p53 mRNA translation in response to UVC-induced DNA damage in breast carcinoma cells. p53 and HuR levels show pulsatile change post UV irradiation. The computed model fitted with the observed pulse of p53 and HuR only when hypothetical regulators of synthesis and degradation of HuR were incorporated. miR-125b, a UV-responsive microRNA, was found to represses the translation of HuR mRNA. Furthermore, UV irradiation triggered proteasomal degradation of HuR mediated by an E3-ubiquitin ligase tripartite motif-containing 21 (TRIM21). The integrated action of miR-125b and TRIM21 constitutes an intricate control system that regulates pulsatile expression of HuR and p53 and determines cell viability in response to DNA damage.

INTRODUCTION

The protein p53 is the hub of a complex regulatory network of incoming stress signals and outgoing effector pathways that plays a crucial tumor suppressor role (Horn and Vousden, 2007). Different stresses such as DNA damage, hypoxia, and oncogene activation upregulate and activate the p53 protein, mainly by inhibiting the interaction between p53 and the E3 ubiquitin ligase Mdm2 (Horn and Vousden, 2007; Michael and Oren, 2003). The enhanced p53 level causes increased Mdm2 expression, which in turn reduces p53 to a low steady-state level, thereby forming a negative feedback loop post DNA damage (Lahav et al., 2004).

Although the core of the p53 regulatory network consists of the p53-Mdm2 negative feedback loop, it is, nevertheless, clear that other mechanisms for regulating p53 protein levels in response to DNA damage are also important. The observation that the protein synthesis inhibitor cycloheximide (CHX) is capable of blocking p53 induction and partially inhibiting G_1 arrest in response to DNA damage provided evidence that the control of p53 mRNA translation plays a key role in p53 induction (Fu et al., 1996; Kastan et al., 1991). Translational regulation of p53 is mediated by the interaction of RNA-binding proteins (RBPs) and microRNAs (miRNAs) with both the 5′ and 3′ UTRs of p53 mRNA (Vilborg et al., 2010). The RBP HuR is a major regulator of p53 mRNA stability and translation in response to DNA damage. HuR undergoes nuclear-cytoplasmic translocation and binds to the p53 mRNA 3′ UTR, enhancing p53 protein synthesis in response to DNA-damaging UVC irradiation (Ahuja et al., 2016; Mazan-Mamczarz et al., 2003).

The first report of an miRNA directly regulating p53 was miR-125b, which is an important negative regulator of p53 protein synthesis and p53-mediated apoptosis (Le et al., 2009). A homolog of miR-125b, miR-125a, also interacts with p53 mRNA 3′ UTR and inhibits translation (Zhang et al., 2009). Recent work has shown that cross talk between miR-125b- and HuR-mediated regulation of p53 mRNA translation controls p53 protein synthesis in response to UV radiation (Ahuja et al., 2016).

Previous studies have shown that the p53 level increases dramatically after exposure to DNA-damaging radiation and then declines in a pulsatile manner (Lev Bar-Or et al., 2000). Interestingly, DNA double-strand breaks, induced by ionizing γ-radiation or radiomimetic drugs such as neocarzinostatin, trigger a series of p53 oscillations with fixed amplitude and duration (Batchelor et al., 2011). In contrast, DNA single-strand

[1]Department of Biological Sciences, Indian Institute of Science Education and Research Kolkata, Mohanpur 741246, West Bengal, India

[2]Department of Chemical Sciences, Indian Institute of Science Education and Research Kolkata, Mohanpur 741246, West Bengal, India

[3]Department of Mathematics and Statistics, Indian Institute of Science Education and Research Kolkata, Mohanpur 741246, West Bengal, India

[4]Proteomics and Metabolomics Core, Lerner Research Institute, Cleveland Clinic, 9500 Euclid Avenue, Cleveland, OH 44195, USA

[5]Department of Physical Sciences, Indian Institute of Science Education and Research Kolkata, Mohanpur 741246, West Bengal, India

[6]Present address: Department of Chemistry and Chemical Biology, Cornell University, Ithaca, NY 14853, USA

[7]Present address: Department of Basic Science & Humanities, Institute of Engineering & Management, Salt Lake Electronics Complex, Kolkata 700091, West Bengal, India

[8]Present address: Department of Biochemistry, Indian Institute of Science, Bangalore 560012, Karnataka, India

[9]Present address: Department of Immunology, H. Lee. Moffitt Cancer Center, MRC-12902 Magnolia Drive, Tampa, FL 33612, USA

[10]These authors contributed equally

[11]These authors contributed equally

Continued

breaks, induced by non-ionizing UV radiation, causes a single pulse of p53, with an amplitude dependent on the UV dose (Batchelor et al., 2011; Collister et al., 1998; Gaglia and Lahav, 2014; Purvis et al., 2012). Moreover, quantitative studies examining p53 expression in individual living cells in response to DNA damage have showed that there is heterogeneity of pulsatile expression of p53 among individual cells in a population (Geva-Zatorsky et al., 2006; Lahav et al., 2004). These observations have introduced new questions regarding the mechanism and function of p53 oscillatory dynamics. A number of studies have employed mathematical modeling approaches to elucidate this behavior (Batchelor et al., 2008; Ma et al., 2005; Proctor and Gray, 2008). All the modeling approaches have only considered the p53-Mdm2 negative feedback loop and its upstream regulators, which regulate p53 protein stability, to explain the oscillatory dynamics of p53 (Ciliberto et al., 2005; Geva-Zatorsky et al., 2006; Lahav, 2008; Lev Bar-Or et al., 2000; Ma et al., 2005; Wagner et al., 2005). However, it is important to consider the regulation of p53 protein synthesis to realistically explain the pulsatile expression pattern of p53 in response to DNA damage. This necessitates the inclusion of regulators of p53 mRNA translation that are induced by DNA damage, such as HuR and miR-125b, in the regulatory model of p53 expression in response to genotoxic stress.

Therefore, to understand the translation regulatory network that controls pulsatile p53 expression in response to DNA damage, we have adopted an approach combining computational modeling and experimental validation in a reiterative manner. We have found that both p53 and HuR levels show a pulse over a 12-h time period after exposure to UV irradiation. However, modeling of the HuR-p53-Mdm2 network failed to show the expression pattern obtained experimentally. Further modeling that fitted the experimental observations suggested the presence of a translation inhibitor and a degradation inducer of HuR. The modeling was validated by the discovery of an miRNA inhibiting translation of HuR mRNA and an E3 ubiquitin ligase inducing HuR protein degradation in response to DNA damage. Together these observations have provided the basis of an approach combining computational modeling and biochemical experimentation, which has allowed the discovery of hitherto unknown regulators of p53 expression in the cellular DNA damage response.

RESULTS

Dynamic Modeling of the Minimal p53-Mdm2 Negative Feedback Circuit Shows a Pulsatile Change in p53 Level

The p53-Mdm2 negative feedback circuit was selected as the minimal network, and a mathematical model of the system dynamics containing the key processes that regulate gene expression was developed. The rate equations representing the expression of p53 and Mdm2 were represented by non-linear differential equations consisting of synthesis and degradation terms. Complete model details, model parameters, and parameter testing are described in Modeling Procedures in Materials and Methods. The numerical integration of the set of differential equations with the parametric values (Table S1) showed a pulsatile change in the p53 level (Figure S1). This suggested that the minimal p53-Mdm2 negative feedback loop was sufficient to explain the oscillatory behavior of p53 expression post DNA damage, as in previous studies (Lahav, 2008; Proctor and Gray, 2008).

Inclusion of HuR and miR-125b as Regulators of p53 Expression Fails to Obtain a Fit between the Model and Experimental Data

The pulsatile change in p53 level corresponded to our experimental observation when we exposed MCF7 breast carcinoma cells to a pulse of UVC radiation and observed a single broad pulse of p53 protein approximately over a period of 12 h post UV exposure (Figure 1A). There was a high positive correlation (Pearson R = 0.68) between the result of the simulation (solid purple line) and the experimental data (bar graphs) obtained from seven independent experiments (Figure S1). However, this feedback circuit only considers the stabilization of p53 and does not consider changes in p53 protein synthesis in response to DNA damage. Therefore HuR and miR-125b were introduced in the model as positive and negative regulators, respectively, of p53 protein synthesis (Figure 1B). Terms representing the effect of HuR and miR-125b were included in the differential rate equation representing p53 expression (Figure 1C). However, in the absence of known regulatory processes for miR-125b expression in response to UV, a curve-fitting equation describing the experimentally observed biphasic miR-125b expression pattern in response to UV was included (Figure 1D) in the model. Remarkably, the simulation of these equations now failed to produce a fit (Pearson R = −0.15) with the experimentally observed pulsatile change in p53 expression (Figure 1E). Moreover, the simulation predicted a linear change in HuR level that did not show any correlation (Pearson R = 0.15) with the experimentally observed change in the cytoplasmic level of HuR, which also

[12]Lead Contact

*Correspondence: psray@iiserkol.ac.in

https://doi.org/10.1016/j.isci.2019.05.002

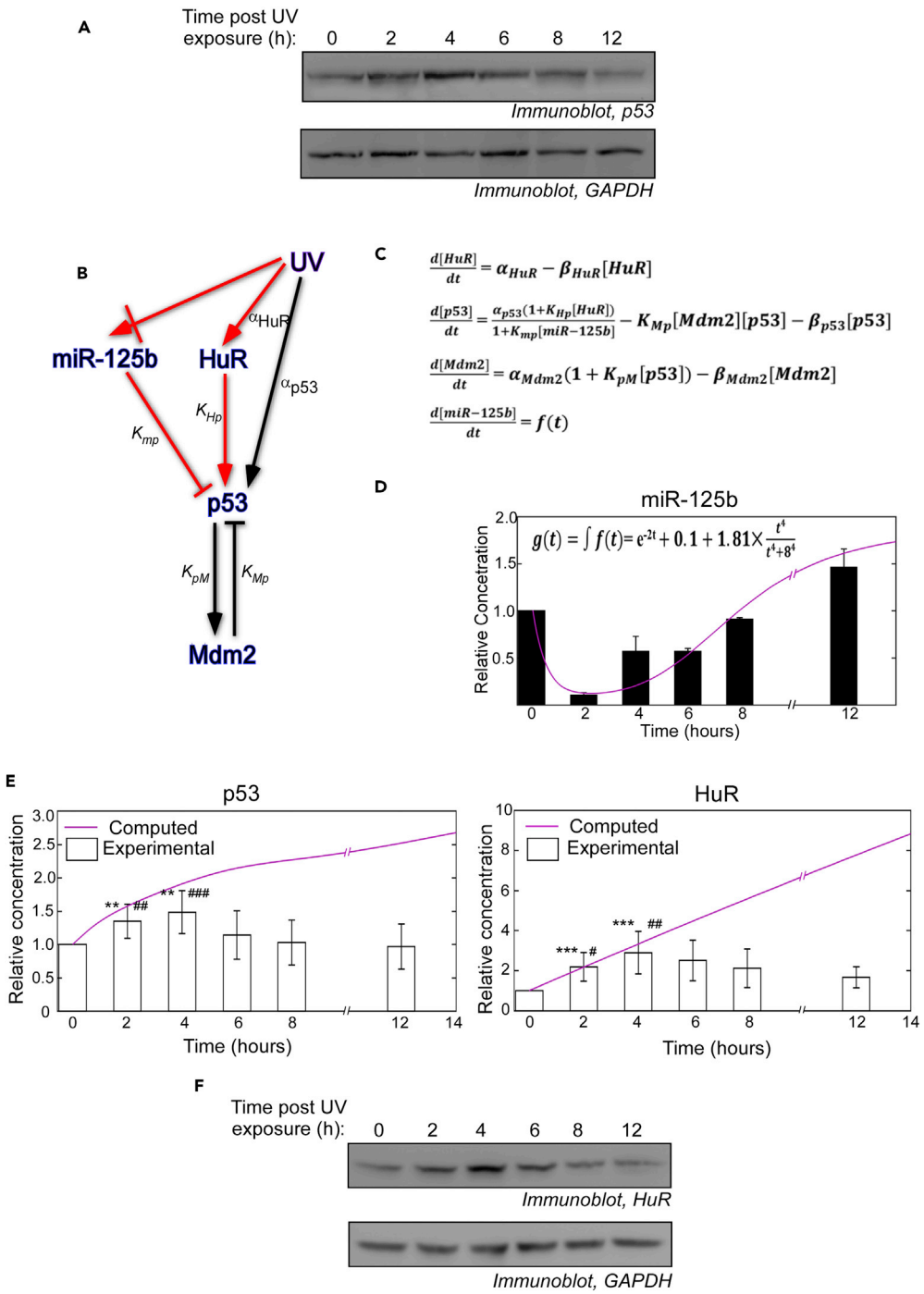

Figure 1. Modeling of the p53 Regulatory Network, Including miR-125b and HuR as Regulators of p53 mRNA Translation, Fails to Obtain a Fit between the Model and Experimental Observations

(A) Representative immunoblot of cytoplasmic lysates of MCF7 cells exposed to a 10 J/m^2 pulse of UVC radiation and collected at indicated time points post UV exposure, probed with p53, and GAPDH antibodies.

(B) Network diagram of the p53 translation regulation network in response to UV irradiation. The edges in red represent newly added regulatory processes.

(C) Rate equations representing the p53 translation regulation network in response to UV irradiation. The rate equation for miR-125b expression consists of a curve-fitting equation with a decreasing exponential function and a Hill equation-like function describing the experimentally observed biphasic miR-125b expression pattern in (C).

Figure 1. *Continued*

(D) Best-fit curve for miR-125b expression over 12-h period post UV irradiation as obtained previously (Ahuja et al., 2016). The curve-fitting equation representing the biphasic expression pattern is represented. The r^2 value for curve fitting of miR-125b expression is 0.918695.

(E) Plots representing simulation and experimental data of change of p53 and HuR levels over a 12-h period post exposure to a 10 J/m^2 pulse of UVC irradiation. The simulation plots (purple lines) represent the numerical integration of the rate equations in (B). The experimental plots (bar graphs) are composed of intensity values of p53 and HuR bands obtained from cell lysates collected at the designated time points post UV exposure. Experimental data represent mean ± SD values from seven independent immunoblots, normalized to corresponding GAPDH band intensities. The normalized band intensities are scaled to the 0-h time point band intensity, taken as 1. * Represents significant difference from values at 0 h, and # represents significant difference from values at 12-h time points. * or # signifies a p-value ≤ 0.05, ** or ## signifies a p-value ≤ 0.01, *** or ### signifies a p-value ≤ 0.005.

(F) Representative immunoblot of cytoplasmic lysates of MCF7 cells exposed to UVC radiation and collected at indicated time points post UV exposure and probed with HuR and GAPDH antibodies.

See also Figures S1 and S13 and Table S1.

showed a broad pulse similar to that of p53 (bar graphs in Figures 1E and 1F). This indicated the potential presence of other, hitherto unknown, regulatory factors induced by DNA damage in the regulatory network regulating p53 expression.

Incorporation of miR-125b as a Negative Regulator of HuR Improves the Model but Does Not Fit with the Experimental Data

The pulsatile change in HuR level in response to UV irradiation suggested the presence of negative regulator(s) of HuR induced by UV radiation. As miR-125b is induced by UV and represses p53 mRNA translation in the same timescale, we considered the possibility of HuR being a target of miR-125b-mediated translation repression. Interestingly, a target site of miR-125b, with a completely complementary seed sequence, was predicted at the 671–692 nucleotide position in the HuR mRNA 3′ UTR by miRNA target prediction algorithms (Figure 2A). miR-125b levels were negatively correlated with HuR levels in the breast carcinoma cell lines MCF7 and MDA-MB-231, and HuR level in MDA-MB-231 cell line was enhanced in a dose-dependent manner by transfection with an antagomiR to miR-125b (Figure S2). Overexpression of miR-125b in MCF7 cells resulted in a dose-dependent decrease in HuR protein level but not in the HuR mRNA level (Figure 2B, quantification in Figure S3A). miR-125b overexpression (Figure S3B) showed a significant dose-dependent decrease in luciferase activity from a reporter gene construct containing the wild-type (WT) HuR 3′ UTR but not from a reporter gene containing the HuR 3′ UTR with a mutant miR-125b target site (Figure 2C). There was no change in firefly luciferase mRNA level on miR-125b overexpression (Figure S3C). Also, transfection of cells overexpressing miR-125b with a miR-125b antagomiR restored luciferase expression from the reporter gene construct containing the HuR 3′ UTR (Figure 2C). UV irradiation of cells transfected with the luciferase reporter constructs showed significant increase of luciferase activity from reporter gene constructs with HuR WT 3′ UTR and HuR 3′ UTR with mutant miR-125b target site at 2 h post UV irradiation, which coincides with the lowest level of miR-125b. However, luciferase activity from the WT 3′ UTR decreased significantly compared with miR-125b target site mutant 3′ UTR at subsequent time points, which coincides with the increase in miR-125b level (Figure S4). Analysis of ribosomal fractions from cells overexpressing miR-125b showed that HuR mRNA was mostly present in the non-translating mRNA-protein complex (mRNP) fractions compared with that in control cells (Figure 2D). HuR mRNA and miR-125b were found to be associated with Ago2, the major component of the RNA-induced silencing complex, by RNA immunoprecipitation of lysates from cells expressing miR-125b (Figure S5). Together, these data established miR-125b as an UV-induced repressor of HuR protein synthesis.

Therefore, we incorporated the miR-125b mediated downregulation of HuR expression in the model of the p53 regulatory network (Figure 2E) with k_{mH} as the regulatory constant representing the effect of miR-125b on HuR expression (Figure 2F). Simulation of the rate equations showed that p53 protein level attained a plateau after the initial increase. Moreover, HuR expression also exhibited a non-linear increase compared with the continuous linear increase as seen in the previous model. However, in neither case the simulation (solid purple line) matched with the experimentally observed change (bar graphs) in protein levels (Pearson R = −0.10 for p53 and 0.21 for HuR) (Figure 2G). Hence inclusion of miR-125b as a negative regulator of HuR protein synthesis improved the model but failed to match the observed pulsatile change in either HuR or p53. This suggested the presence of yet unknown regulatory factor(s) in the network.

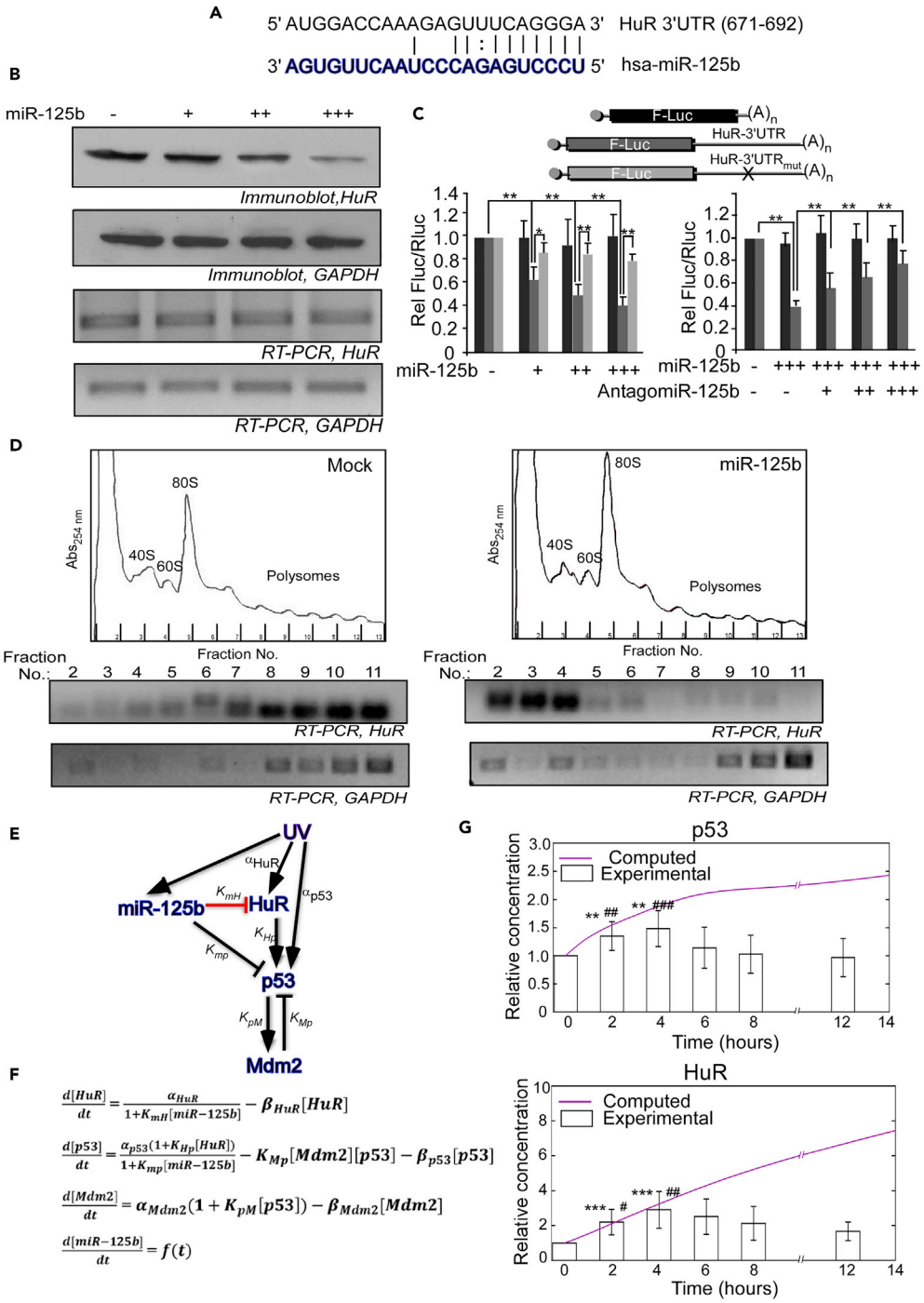

Figure 2. Inclusion of miR-125b As a Negative Regulator of HuR Expression Fails to Obtain a Fit between the Model and Experimental Observations

(A) Schematic representation of the region of the HuR 3′ UTR containing the putative miR-125b target site and *Homo sapiens* miR-125b sequence.

(B) Immunoblots of lysates of MCF7 cells transfected with three increasing concentrations of pSUPER-EGFP-miR-125b probed with HuR and GAPDH antibodies. Semiquantitative RT-PCR of total RNA isolated from the cell lysates using HuR- and GAPDH-specific primers (lower panels).

(C) MCF7 cells transfected with firefly luciferase constructs without 3′ UTR sequence or containing HuR-WT mRNA 3′ UTR or miR-125b-binding-site-mutated HuR mRNA 3′ UTR were cotransfected with three increasing concentrations of

Figure 2. *Continued*

pSUPER-miR-125b (left panel). MCF7 cells transfected with firefly luciferase constructs without 3′ UTR sequence or containing HuR-WT mRNA 3′ UTR were cotransfected with the highest concentration of pSUPER-miR-125b and three increasing concentrations of antagomiR-125b (right panel). Fluc values are normalized to Rluc values as transfection control. Data represent mean ± SD values from three independent experiments, each with two technical replicates. The normalized band intensities are scaled to the control lacking miR-125b, taken as 1. * signifies a p-value ≤ 0.05, ** signifies a p-value ≤ 0.01.

(D) Ribosomal fractions from MCF7 cells, either mock transfected or transfected with pSUPER-miR-125b, were analyzed by sucrose density gradient fractionation. Ribosomal RNA content, measured at 254 nm, is plotted against fraction numbers. RNA isolated from selected fractions was analyzed by semi-quantitative RT-PCR using HuR and GAPDH primers.

(E) Network diagram of the p53 translation regulation network in response to UV irradiation. The edge in red represents newly added regulatory process.

(F) Rate equations representing the p53 translation regulation network in response to UV irradiation. The rate equation for HuR expression contains a term representing the effect of miR-125b (K_{mH}) on HuR synthesis. Other equations are as earlier.

(G) Plots representing simulation and experimental data of change of p53 and HuR levels over a 12-h period post exposure to a 10-J/m^2 pulse of UVC irradiation. The simulation plot represents the numerical integration of the rate equations in (F). The experimental graphs are as earlier. * Represents significant difference from values at 0 h, and # represents significant difference from values at 12-h time point. * or # signifies a p-value ≤ 0.05, ** or ## signifies a p-value ≤ 0.01, *** or ### signifies a p-value ≤ 0.005.

See also Figures S2–S5 and S14 and Table S1.

Incorporation of a Hypothetical Protein Degradation Factor as a Negative Regulator of HuR in the Model Obtains a Fit with the Experimental Data

Incorporation of miR-125b as an inhibitor of HuR protein synthesis in the model only modified the nature of the expression kinetics but failed to match the pulsatile expression pattern of HuR. We therefore investigated whether the degradation of HuR protein contributed to the pulsatile change in HuR level. HuR protein level was found to remain nearly unaltered for 12 h in cells treated with CHX, an inhibitor of global protein synthesis, demonstrating HuR to be a highly stable protein (Figure 3A, quantification in Figure S6A). However, UV irradiation with CHX treatment led to a 70% reduction in HuR protein by 12 h, suggesting a rapid degradation of HuR protein induced by UV exposure (Figure 3A, quantification in Figure S6B). Therefore we investigated whether UV induced proteasomal degradation of HuR. Treatment of cells with CHX and MG-132, a proteasome inhibitor, prevented the degradation of HuR post UV exposure (Figure 3A, quantification in Figure S6C). Also, immunoprecipitation of HuR, followed by western blot with anti-ubiquitin antibody, showed enhanced poly-ubiquitination of HuR in UV-treated cells when compared with cells not exposed to UV (Figure 3B). The poly-ubiquitination of HuR increased in a time-dependent manner and showed a maximum between 6 and 12 h post UV exposure, coinciding with the decrease in HuR level (Figure 3C). Together, these observations demonstrated that HuR undergoes ubiquitination and proteasomal degradation induced by UV irradiation.

As no regulator of HuR degradation in response to UV irradiation was known, we postulated "X" as a novel negative regulator of HuR that is induced as a result of UV irradiation and leads to degradation of HuR protein (Figure 3D). X was incorporated as a negative regulator of HuR in the differential equation describing the expression of HuR (Figure 3E). Remarkably, simulation of the rate equations generated a pulsatile expression pattern for both p53 and HuR (solid purple lines), which matched satisfactorily (Pearson R = 0.76 for p53 and R = 0.94 for HuR) with the experimentally observed change in HuR and p53 levels (bar graphs) post DNA damage (Figure 3F). This suggested that the pulsatile change in HuR level, and its effect on p53, may be a result of the combination of translation repression of HuR mRNA by miR-125b and degradation of HuR protein by an unknown factor(s) induced by UV radiation.

The Hypothetical HuR Degradation Factor "X" Is the E3 Ubiquitin Ligase TRIM21

To identify the hypothetical HuR protein degradation factor "X," myc-tagged HuR was overexpressed in MCF7 cells. Cells exposed to UV irradiation and treated with MG132 were lysed 6 h after UV exposure, and lysates were immunoprecipitated with anti-HuR antibody and IgG. The immunoprecipitate was analyzed by mass spectrometry for proteins specifically co-immunoprecipitated with HuR when compared with IgG (Table S2). Two proteins, Serpin B3 and the E3 ubiquitin protein ligase tripartite motif-containing 21 (TRIM21), along with HuR itself, were found to be specifically present in the HuR immunoprecipitate. Serpin B3 was not considered to play a role in HuR degradation as it is a serine protease inhibitor. However, as HuR was found to undergo proteasomal degradation in response to UV irradiation, interaction with an E3

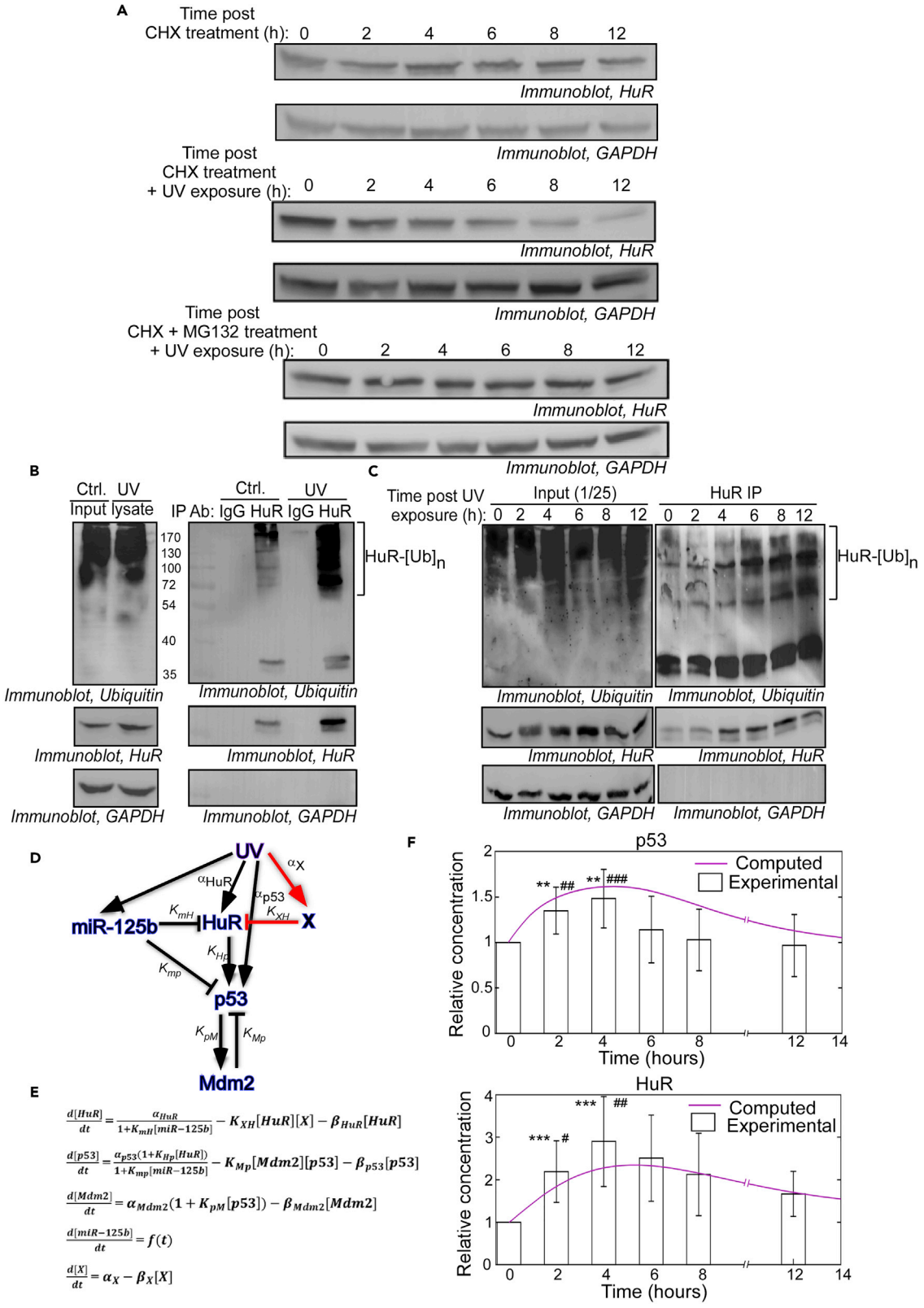
A
Time post CHX treatment (h): 0 2 4 6 8 12
Immunoblot, HuR
Immunoblot, GAPDH
Time post CHX treatment + UV exposure (h): 0 2 4 6 8 12
Immunoblot, HuR
Immunoblot, GAPDH
Time post CHX + MG132 treatment + UV exposure (h): 0 2 4 6 8 12
Immunoblot, HuR
Immunoblot, GAPDH
B
Ctrl. UV
Input lysate
IP Ab: IgG HuR IgG HuR
170
130
100
72
54
40
35
HuR-[Ub]n
Immunoblot, Ubiquitin
Immunoblot, HuR
Immunoblot, GAPDH
C
Time post UV exposure (h): Input (1/25) 0 2 4 6 8 12
HuR IP 0 2 4 6 8 12
HuR-[Ub]n
Immunoblot, Ubiquitin
Immunoblot, HuR
Immunoblot, GAPDH
D
UV
αX
αHuR
αp53
KmH
KXH
miR-125b
HuR
X
KHp
Kmp
p53
KpM
KMp
Mdm2
E
$\frac{d[HuR]}{dt} = \frac{\alpha_{HuR}}{1+K_{mH}[miR-125b]} - K_{XH}[HuR][X] - \beta_{HuR}[HuR]$
$\frac{d[p53]}{dt} = \frac{\alpha_{p53}(1+K_{Hp}[HuR])}{1+K_{mp}[miR-125b]} - K_{Mp}[Mdm2][p53] - \beta_{p53}[p53]$
$\frac{d[Mdm2]}{dt} = \alpha_{Mdm2}(1 + K_{pM}[p53]) - \beta_{Mdm2}[Mdm2]$
$\frac{d[miR-125b]}{dt} = f(t)$
$\frac{d[X]}{dt} = \alpha_X - \beta_X[X]$
F
p53
Computed
Experimental
** ## ** ###
Relative concentration
Time (hours)
HuR
Computed
Experimental
*** # *** ##
Relative concentration
Time (hours)

Figure 3. Inclusion of a Hypothetical Protein Degradation Factor As a Negative Regulator of HuR Obtains a Fit between the Model and Experimental Observations

(A) Immunoblots of lysates of MCF7 cells treated with cycloheximide (CHX) (upper panels), CHX and UV irradiation (middle panels), or CHX, MG132, and UV irradiation (lower panels) and collected at designated time points over a 12-h period. Lysates were probed with HuR and GAPDH antibodies.

(B) Lysates of MCF7 cells not exposed (Ctrl.) or exposed to UV irradiation and treated with MG132 were immunoprecipitated with HuR antibody or non-immune IgG, and the immunoprecipitates probed with ubiquitin (upper panel), HuR (middle panel), and GAPDH (lower panel) antibodies. Left panels represent the input lysates probed with the same antibodies.

(C) Lysates of MCF7 cells exposed to UV irradiation and treated with MG132 were collected at designated time point over a 12-h period post UV exposure and immunoprecipitated with HuR antibody and the immunoprecipitates probed with ubiquitin (upper panel), HuR (middle panel), and GAPDH (lower panel) antibodies. Left panels represent the input lysates probed with the same antibodies.

(D) Network diagram of the p53 translation regulation network in response to UV irradiation. The edges in red represent newly added regulatory processes.

(E) Rate equations representing the p53 translation regulation network in response to UV irradiation. The rate equation for HuR expression contains a term representing the effect of X (K_{XH}) on HuR degradation. α_X and β_X are assumed parameters representing rates of synthesis and degradation, respectively, of X. Other equations are as earlier.

(F) Plots representing simulation and experimental data of change of p53 and HuR levels over a 12-h period post exposure to a 10-J/m^2 pulse of UVC irradiation. The simulation plot (purple line) represents the numerical integration of the rate equations in (E). The experimental graphs are as earlier.

* Represents significant difference from values at 0 h, and # represents significant difference from values at 12-h time points. * or # signifies a p-value $\leq$ 0.05, ** or ## signifies a p-value $\leq$ 0.01, *** or ### signifies a p-value $\leq$ 0.005.

See also Figures S6 and S15 and Table S1.

ubiquitin ligase was highly significant. Therefore the E3 ubiquitin ligase TRIM21 was considered as a potential candidate for the unknown factor "X."

TRIM21 Interacts with HuR in Response to UV Irradiation and Causes Poly-ubiquitination and Degradation of HuR

To confirm the interaction between TRIM21 and HuR, TRIM21 was immunoprecipitated from MCF7 cells treated with MG132, and HuR was found to associate with TRIM21 by immunoblotting with HuR antibody, and vice versa (Figure 4A). This interaction between HuR and TRIM21 was found to be enhanced in UV-exposed cells when compared with cells not exposed to UV (Figure 4B) and was independent of RNA binding (Figure S7). Also, the interaction between TRIM21 and HuR was found to increase in a time-dependent manner over the period of 12 h post UV exposure and was maximum between 4 and 12 h post UV exposure, which coincided with the previously observed decrease in HuR level (Figure 4C). We also checked whether the knockdown of TRIM21 affected the poly-ubiquitination of HuR post UV irradiation. Cells transfected with a small interfering RNA (siRNA) against TRIM21 (Figure 4D, lower panel) showed reduced poly-ubiquitination of HuR post UV exposure, compared with cells transfected with a control siRNA, and the level of poly-ubiquitination of HuR in siTRIM21-transfected cells exposed to UV was similar to that in cells not exposed to UV (Figure 4D, right panel, lanes 1 and 4). Overexpression of TRIM21 in MCF7 cells caused the degradation of HuR upon UV irradiation only, confirming that UV irradiation induced the interaction between TRIM21 and HuR and the subsequent degradation of the latter (Figure 4E). The breast carcinoma cell line MDA-MB-231, which has lower level of HuR compared with MCF7, was found to have higher level of TRIM21, and siRNA-mediated knockdown of TRIM21 in MDA-MB-231 could enhance the level of HuR in these cells (Figure 4F). Together, these observations showed TRIM21 as the E3 ubiquitin ligase responsible for the UV-induced poly-ubiquitination and degradation of HuR.

UV-Induced Ubiquitination of Lys-182 by TRIM21 Causes HuR Degradation

Previously ubiquitination of the Lys-182 (K182) residue in the RNA recognition motif 2 (RRM2) of HuR (Figure 5A) has been shown to be responsible for HuR degradation induced by heat shock, but the E3 ubiquitin ligase that ubiquitinates the K182 residue was not demonstrated (Abdelmohsen et al., 2009). Therefore we investigated whether the UV-induced degradation of HuR involved ubiquitination of K182 and TRIM21 was the E3 ubiquitin ligase responsible. Exogenous expression of Myc-tagged wild-type HuR (HuR-WT) and HuR in which the Lys-182 was mutated to Arg (K182R) in MCF7 cells followed by UV irradiation led to degradation of HuR-WT during the 12-h period post UV irradiation, whereas HuR-K182R was refractory to degradation (Figure 5B). Determination of the half-life of the WT and K182R mutant HuR post UV-irradiation showed that HuR-WT had a half-life of around 7 h, whereas the half-life of the K182R mutant was greater than 12 h (Figure 5C). Overexpression of hemagglutinin (HA)-tagged ubiquitin in cells showed a 2-fold decrease in HuR level compared with cells not overexpressing ubiquitin 6 h post UV exposure (Figure S8). Cells expressing HA-tagged ubiquitin, when transfected with constructs expressing HuR-WT or K182R mutant HuR and exposed to UV, showed significantly higher ubiquitination of HuR-WT compared with K182R mutant HuR (Figure 5D). The overall level of ubiquitination remained nearly unchanged in cells

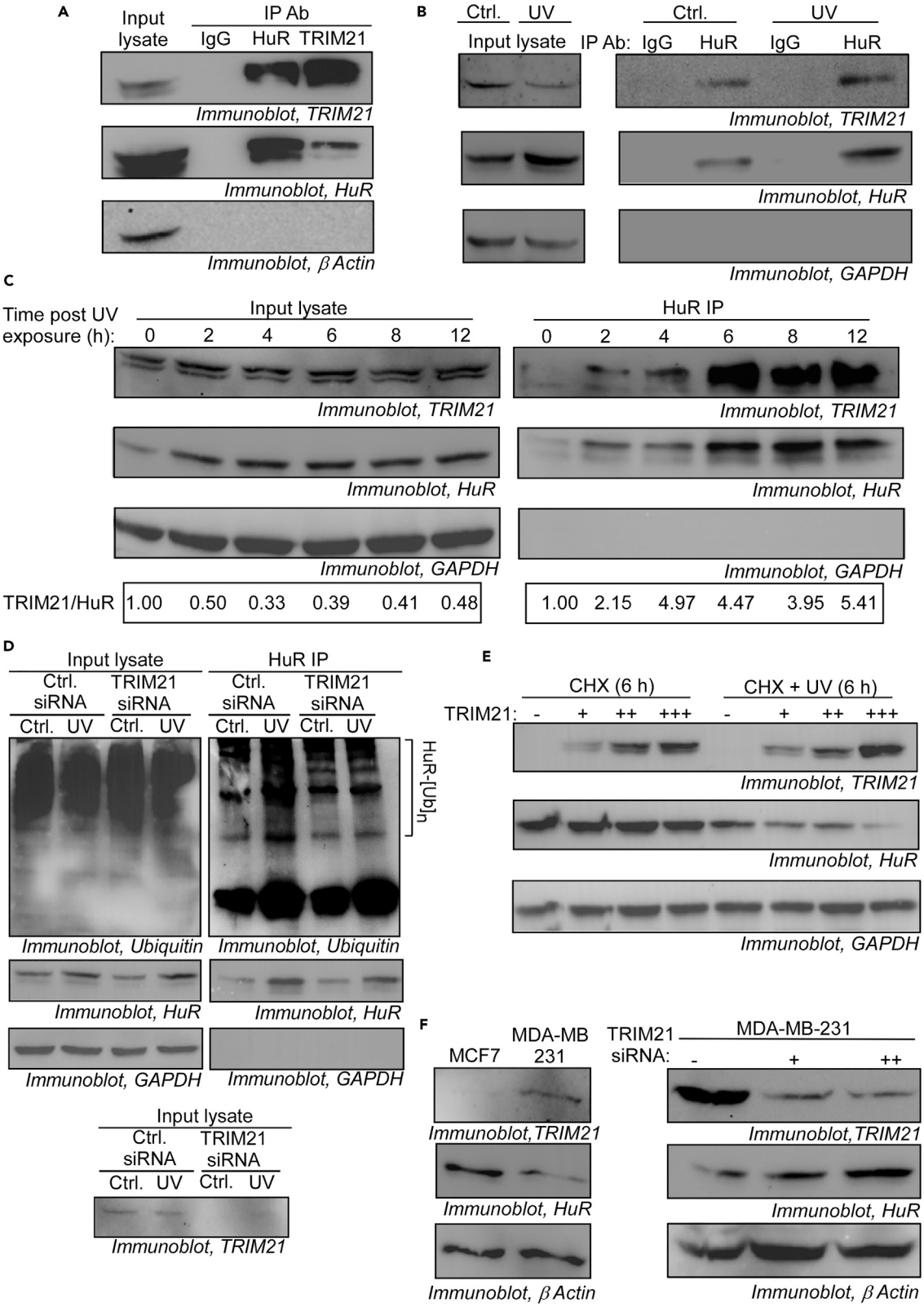
A
Input lysate
IP Ab
IgG
HuR
TRIM21
Immunoblot, TRIM21
Immunoblot, HuR
Immunoblot, β Actin
B
Ctrl.
UV
Input lysate
IP Ab:
IgG
HuR
Immunoblot, TRIM21
Immunoblot, HuR
Immunoblot, GAPDH
C
Time post UV exposure (h):
Input lysate
HuR IP
0 2 4 6 8 12
Immunoblot, TRIM21
Immunoblot, HuR
Immunoblot, GAPDH
TRIM21/HuR
1.00 0.50 0.33 0.39 0.41 0.48
1.00 2.15 4.97 4.47 3.95 5.41
D
Input lysate
HuR IP
Ctrl. siRNA
TRIM21 siRNA
Ctrl. UV Ctrl. UV
HuR-[Ub]n
Immunoblot, Ubiquitin
Immunoblot, HuR
Immunoblot, GAPDH
Input lysate
Ctrl. siRNA
TRIM21 siRNA
Ctrl. UV Ctrl. UV
Immunoblot, TRIM21
E
CHX (6 h)
CHX + UV (6 h)
TRIM21:
- + ++ +++ - + ++ +++
Immunoblot, TRIM21
Immunoblot, HuR
Immunoblot, GAPDH
F
MCF7
MDA-MB 231
Immunoblot, TRIM21
Immunoblot, HuR
Immunoblot, β Actin
TRIM21 siRNA:
MDA-MB-231
- + ++
Immunoblot, TRIM21
Immunoblot, HuR
Immunoblot, β Actin

Figure 4. TRIM21 Causes Poly-ubiquitination and Degradation of HuR in Response to UV Irradiation

(A) MCF7 cell lysates, treated with MG132, were immunoprecipitated with HuR antibody and immunoblotted with TRIM21 antibody, and vice versa. Non-immune IgG was used as control antibody for immunoprecipitation.

(B) Lysates of MCF7 cells not exposed (Ctrl.) or exposed to UV irradiation, and treated with MG132, were immunoprecipitated with HuR antibody or non-immune IgG and the immunoprecipitates probed with TRIM21 (upper panel), HuR (middle panel), and GAPDH (lower panel) antibodies. Left panels represent the input lysates probed with the same antibodies.

(C) Lysates of MCF7 cells exposed to UV irradiation and treated with MG132 were collected at designated time points over a 12-h period post UV exposure and immunoprecipitated with HuR antibody, and the immunoprecipitates probed with TRIM21 (upper panel), HuR (middle panel), and GAPDH (lower panel) antibodies. Left panels represent the input lysates probed with the same antibodies. The ratio between TRIM21 and HuR band intensities are shown in boxes below left and right panels.

(D) MCF7 cells transfected with control siRNA or siRNA against TRIM21 were not exposed (Ctrl.) or exposed to UV irradiation and treated with MG132. Cell lysates were immunoprecipitated with HuR antibody, and the immunoprecipitates probed with ubiquitin (upper panel), HuR (middle panel), and GAPDH (lower panel) antibodies. Left panels represent the input lysates probed with the same antibodies. The bottom panel represents the input lysates (transfected with Ctrl. siRNA and TRIM21 siRNA) probed with TRIM21 antibody.

(E) MCF7 cells transfected with three increasing concentrations of a TRIM21-expressing vector were treated with CHX and not exposed or exposed to UV irradiation. Cells were collected 6 h after UV exposure, and lysates were immunoblotted with TRIM21 (upper panel), HuR (middle panel), and GAPDH (lower panel) antibodies.

(F) Lysates from MCF7 and MDA-MB-231 cells were immunoblotted with TRIM21 (upper panel), HuR (middle panel), and β-actin (lower panel) antibodies (left panels). Lysates from MDA-MB-231 cells transfected with increasing concentrations of TRIM21 siRNA were immunoblotted with TRIM21 (upper panel), HuR (middle panel), and GAPDH (lower panel) antibodies (right panels).

See also Figure S7 and Table S2.

expressing HuR-WT or K182R mutant HuR. Overexpression of TRIM21 in cells expressing wild-type or K182R mutant HuR showed reduced interaction of TRIM21 with K182R mutant HuR post UV irradiation (Figure 5E). Also, overexpression of TRIM21 showed reduced degradation of K182R mutant HuR compared with HuR-WT in a dose-dependent manner 6 h post UV irradiation (Figure 5F, quantification in Figure S9A). Finally, the K182R mutant HuR failed to show the decrease in level 12 h post UV irradiation after the increase at 4 h, as observed for HuR-WT (Figure 5G, quantification in Figure S9B). Together, these observations demonstrate Lys-182 residue of HuR as the target of TRIM21-mediated degradation of HuR post UV irradiation.

The UV-Induced Pulse of HuR and p53 Is Abolished with Knockdown of TRIM21

To validate TRIM21 as the E3 ubiquitin ligase contributing to the pulsatile change in HuR and p53 levels in response to UV irradiation, cells were transfected with an siRNA against TRIM21 to repress TRIM21 expression. Cells transfected with control siRNA followed by UV exposure showed a pulsatile change in cytoplasmic HuR level as observed earlier (Figure 6A). HuR level became highest at 4 h and gradually decreased thereafter till 12 h. However, cytoplasmic HuR showed an initial increase at 2 h in TRIM21 knockdown lysates and remained constant thereafter till 8–12 h post UV exposure. p53 also showed a pulsatile expression pattern in control siRNA-treated cells, which was abolished with TRIM21 knockdown resulting in a sustained high level of p53 (Figure 6A). To investigate the effect of TRIM21 on HuR degradation, cells transfected with siRNA against TRIM21 or control siRNA were treated with CHX followed by UV irradiation. Immunoblotting of the whole-cell lysate with anti-HuR antibody showed that the HuR level started to decrease from 2 h onward and showed a significant reduction by 12 h in the control siRNA-transfected cells (Figure S10). However, HuR levels remained nearly constant post UV exposure in TRIM21 knockdown cells. These observations demonstrated that the pulsatile change of both HuR and p53 in response to UV irradiation is abolished with knockdown of TRIM21, hence confirming TRIM21 as the E3 ubiquitin ligase involved in HuR degradation and consequently regulating the pulsatile expression of p53.

Integrated Regulation of HuR by miR-125b and TRIM21 Gives Rise to the Pulsatile Change in HuR and p53 Levels and Regulates Cell Viability in Response to UV

The modeling of p53 and HuR expression post UV-mediated DNA damage led to the discovery of miR-125b and TRIM21 as regulators of HuR synthesis and degradation, respectively. We therefore investigated the combined contributions of miR-125b and TRIM21 in generating the pulsatile change of cytoplasmic HuR and p53 levels in response to UV irradiation. MCF7 cells treated with a control oligo showed the pulsatile pattern of cytoplasmic HuR during the 12-h period post UV irradiation with a peak at around 4 h post UV exposure (Figure 6B). However, treatment with an antagomiR against miR-125b abolished the pulse and resulted in a plateau in HuR level from around 6 h post UV exposure (Figure 6B and best-fit curve in Figure 6C). This demonstrated that antagonizing miR-125b function resulted in de-repression of HuR protein synthesis. Similarly, inhibition of HuR degradation by siRNA-mediated knockdown of TRIM21 resulted in a

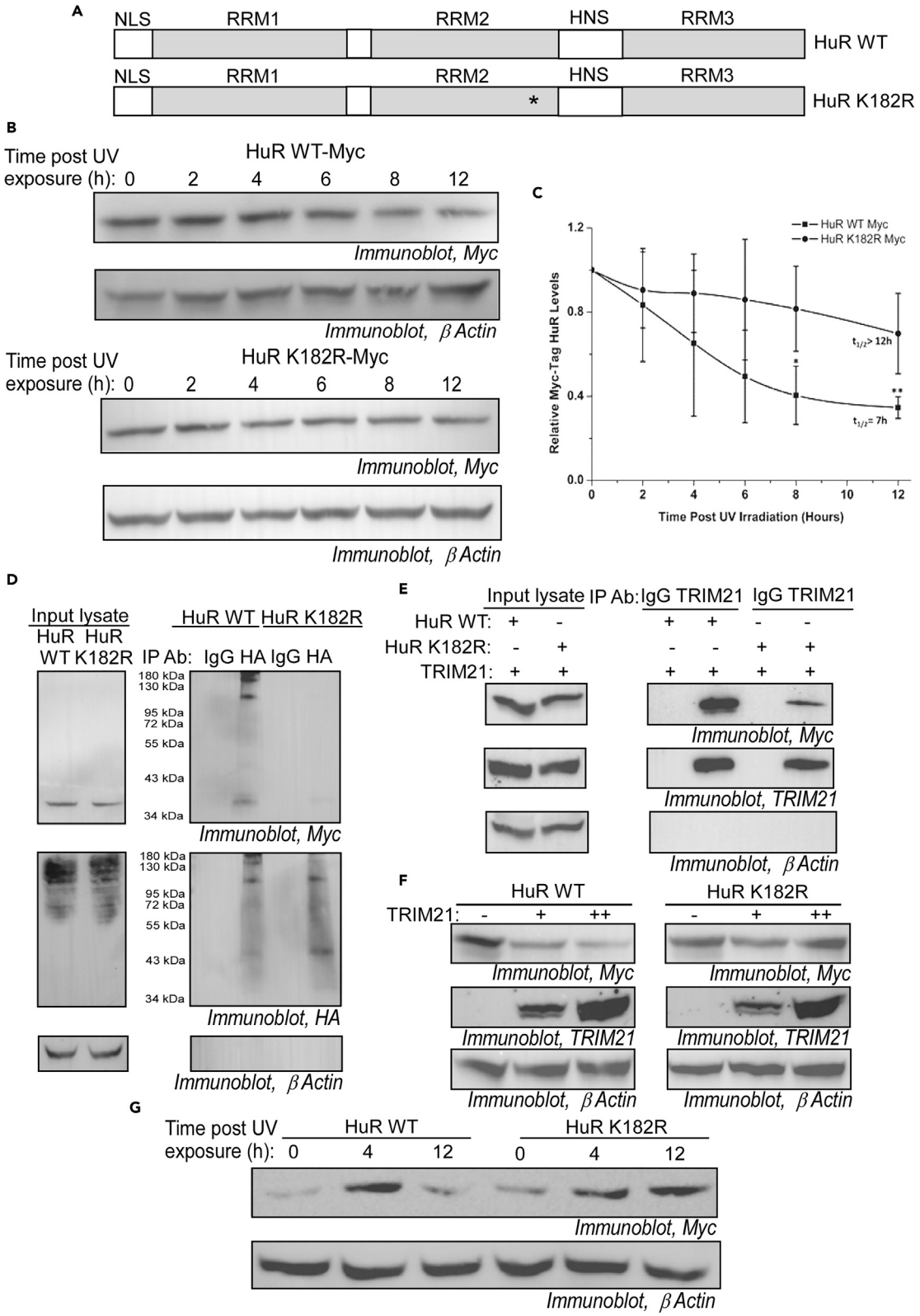
A
NLS
RRM1
RRM2
HNS
RRM3
HuR WT
NLS
RRM1
RRM2
HNS
RRM3
*
HuR K182R
B
Time post UV exposure (h): 0 2 4 6 8 12
HuR WT-Myc
Immunoblot, Myc
Immunoblot, β Actin
Time post UV exposure (h): 0 2 4 6 8 12
HuR K182R-Myc
Immunoblot, Myc
Immunoblot, β Actin
C
HuR WT Myc
HuR K182R Myc
Relative Myc-Tag HuR Levels
1.2
0.8
0.4
0.0
t1/2> 12h
t1/2= 7h
*
**
0 2 4 6 8 10 12
Time Post UV Irradiation (Hours)
D
Input lysate
HuR WT
HuR K182R
HuR WT HuR K182R
IP Ab: IgG HA IgG HA
180 kDa
130 kDa
95 kDa
72 kDa
55 kDa
43 kDa
34 kDa
Immunoblot, Myc
Immunoblot, HA
Immunoblot, β Actin
E
Input lysate
IP Ab: IgG TRIM21 IgG TRIM21
HuR WT: + - + + - -
HuR K182R: - + - - + +
TRIM21: + + + + + +
Immunoblot, Myc
Immunoblot, TRIM21
Immunoblot, β Actin
F
HuR WT
HuR K182R
TRIM21: - + ++ - + ++
Immunoblot, Myc
Immunoblot, Myc
Immunoblot, TRIM21
Immunoblot, TRIM21
Immunoblot, β Actin
Immunoblot, β Actin
G
Time post UV exposure (h): HuR WT 0 4 12 HuR K182R 0 4 12
Immunoblot, Myc
Immunoblot, β Actin

Figure 5. UV-Induced Ubiquitination of Lys-182 by TRIM21 Causes HuR Degradation

(A) Schematic diagram of the HuR wild-type (HuR WT) and Lys-182 to Arg mutant HuR (HuR K182R). * Indicates the position of K182 to R mutation.

(B) Immunoblots of lysates of MCF7 cells transfected with Myc-tagged HuR WT (upper panel) and HuR K182R (lower panel) expression constructs, treated with cycloheximide and UV irradiated, and collected at designated time points over a 12-h period post UV irradiation. Lysates were probed with Myc and β-actin antibodies.

(C) Quantification of Myc-tagged HuR levels from cells expressing HuR WT and HuR K182R over a 12-h period post UV irradiation. Data represent mean ± SD values from three independent experiments. *$p \leq 0.05$, **$p \leq 0.01$ between corresponding time points.

(D) Cells-expressing Myc-tagged HuR WT or HuR K182R were transfected with a construct expressing HA-ubiquitin. At 36 h post transfection cells were treated with MG132 and UV irradiated. Lysates from cells collected 6 h post UV irradiation were immunoprecipitated with anti-hemagglutinin (HA) or control IgG antibodies. Immunoprecipitates and input lysates were immunoblotted with anti-Myc, anti-HA, and anti-β-actin antibodies.

(E) Cells expressing Myc-tagged HuR WT or HuR K182R were transfected with a construct expressing TRIM21. At 48 h post transfection cells were treated with MG132 and UV irradiated. Lysates from cells collected 6 h post UV irradiation were immunoprecipitated with anti-TRIM21 or control IgG antibodies. Immunoprecipitates and input lysates were immunoblotted with anti-Myc, anti-TRIM21, and anti-β-actin antibodies.

(F) Cells expressing Myc-tagged HuR WT or HuR K182R were transfected with three increasing concentrations of a construct expressing TRIM21. At 48 h post transfection cells were treated with CHX for 30 min and UV irradiated. Lysates from cells collected 6 h post UV irradiation were immunoblotted with anti-Myc, anti-TRIM21, and anti-β-actin antibodies.

(G) Cells expressing Myc-tagged HuR WT or HuR K182R were UV irradiated. Cytoplasmic lysates from cells collected 4 and 12 h after UV irradiation were immunoblotted with anti-Myc and anti-β-actin antibodies.

See also Figures S8 and S9.

plateau in HuR level from around 6 h post UV exposure (Figure 6B and best-fit curve in Figure 6C). Remarkably, the combination of antagomiR against miR-125b and the siRNA against TRIM21 resulted in a linear increase in HuR level during the 12 h post UV irradiation (Figure 6B and best-fit curve in Figure 6C). This demonstrated that the combination of translation de-repression and inhibition of degradation converted the pulsatile expression pattern of HuR post DNA damage to a linear increase, as seen in our initial model (Figure 1E). Similar effects of antagomiR-125b and TRIM21 siRNA were observed on p53 levels, except that upon treatment with combination of antagomiR-125b and TRIM21 siRNA, p53 level attained a plateau unlike HuR level (Figure 6B and best-fit curve in Figure 6C). This is likely due to the effect of Mdm2-mediated degradation of p53, which continues to operate during this time period and counteracts the de-repression of p53 protein synthesis. Also, removal of miR-125b from the model, with the retention of the degradation factor, resulted in both p53 and HuR levels attaining plateaux (Figure S11), corresponding to the experimental observations on antagomiR-125b transfection. This shows that the abrogation of either translation repression or protein degradation will result in the loss of the pulsatile change in HuR and p53 levels.

To investigate the effect of the miR-125b-TRIM21-HuR-p53 regulatory network on cell behavior in response to DNA damage, we checked the viability of the UV-treated cells, which have been subjected to inhibition of miR-125b or TRIM21 function, or both. Prolonged increase in p53 level in response to DNA damage will block the cell cycle and decrease cell viability, whereas the pulsatile decrease in p53 level will allow the cells to re-enter the cell cycle and resume cell proliferation. Analysis of the viability of UV-treated MCF7 cells showed that cells transfected with a control oligo did not show a significant change in cell viability, except at 4 h post UV treatment, when the p53 level is the highest (Figure 7A). However, cells that have been transfected with either antagomiR-125b or TRIM21 siRNA or both, in all of which cases p53 levels attains a high plateau from 8–12 h post UV treatment, showed significant reduction in cell viability when compared with control oligo-transfected cells (Figure 7A). We also checked whether the change in cell viability on treatment with antagomiR-125b or TRIM21 siRNA was due to the effect of changes in p53 level. MDA-MB-231 cells, which have non-functional p53, were similarly transfected with a control oligo, antagomiR-125b or TRIM21 siRNA, or a combination of both. Interestingly, MDA-MB-231 cells transfected with control oligo showed significantly reduced viability from 8–12 h post UV irradiation, suggesting that the absence of DNA repair activity of p53 in these cells led to reduced viability (Figure 7B). Also, there was no difference in viability between cells treated with the control oligo and with antagomiR-125b or TRIM21 siRNA or both, unlike in MCF7 cells, indicating that the absence of functional p53 resulted in no effect of inactivation of miR-125b and TRIM21 (Figure 7B). These observations demonstrated that the crucial effect of the miR-125b-TRIM21-HuR regulatory network on cell survival is mediated by its effect on the regulation of p53 expression.

DISCUSSION

Dynamic modeling, coupled with experimental validation, of the regulatory system controlling p53 mRNA translation in response to UV-induced DNA damage revealed the role of miR-125b and TRIM21 as regulators of protein synthesis and degradation, respectively, of the RNA-binding protein HuR. HuR undergoes nuclear-cytoplasmic translocation in response to a variety of stress stimuli such as UV, bacterial

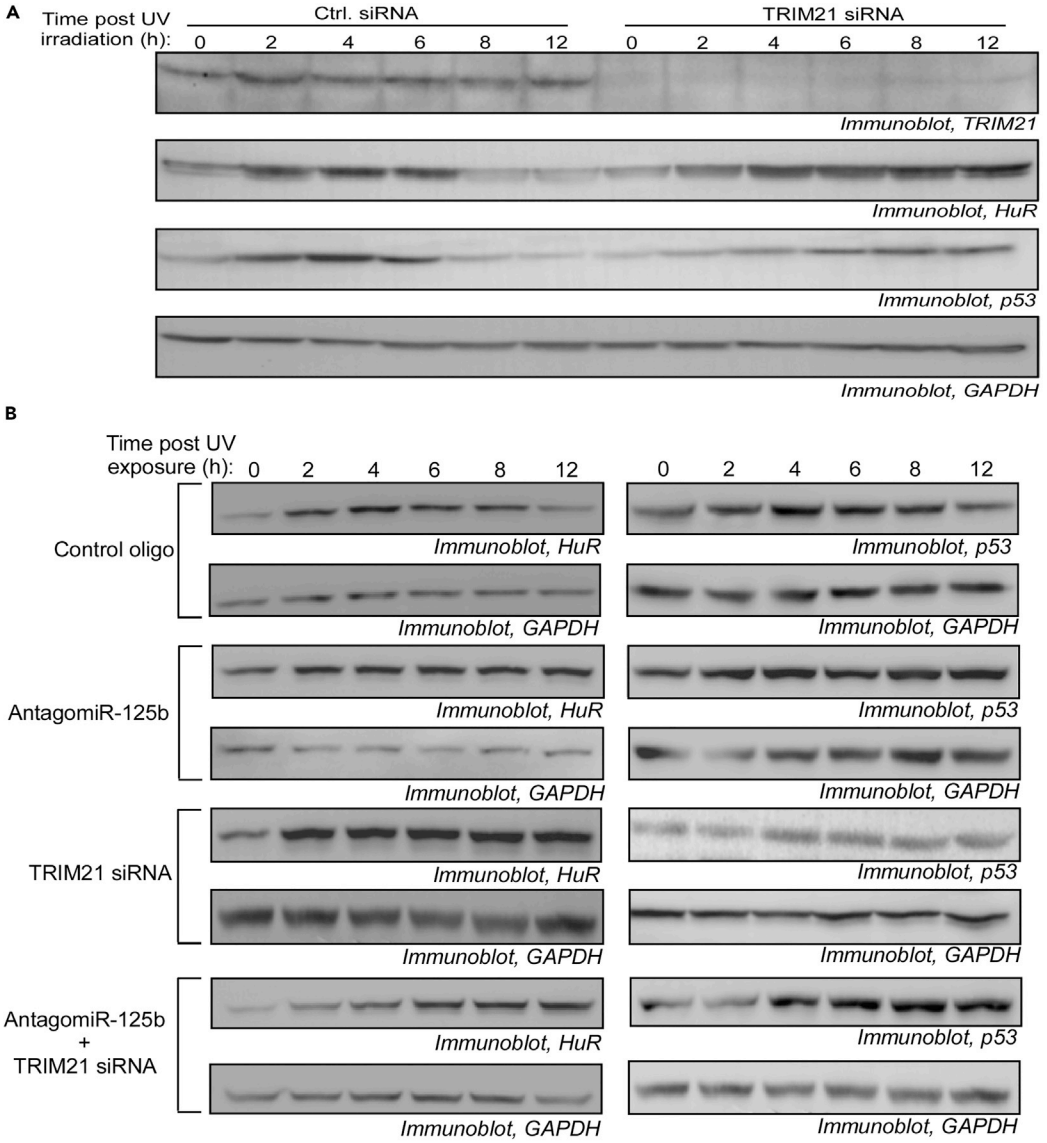
A
Time post UV irradiation (h):
Ctrl. siRNA
TRIM21 siRNA
0 2 4 6 8 12 0 2 4 6 8 12
Immunoblot, TRIM21
Immunoblot, HuR
Immunoblot, p53
Immunoblot, GAPDH
B
Time post UV exposure (h): 0 2 4 6 8 12 0 2 4 6 8 12
Control oligo
AntagomiR-125b
TRIM21 siRNA
AntagomiR-125b + TRIM21 siRNA
Immunoblot, HuR
Immunoblot, p53
Immunoblot, GAPDH
C
Control oligo
AntagomiR-125b
TRIM21 siRNA
AntagomiR-125b + TRIM21 siRNA
Relative HuR level
Relative p53 level
Time post UV exposure (h)
Time post UV exposure (h)

Figure 6. Integrated Regulation of HuR by miR-125b and TRIM21 Contributes to the Pulsatile Change in HuR and p53 Levels in Response to UV Irradiation

(A) Cytoplasmic lysates of MCF7 cells transfected with control siRNA or TRIM21 siRNA and exposed to UV irradiation were collected at designated time points post UV exposure and immunoblotted with TRIM21, HuR, p53, and GAPDH antibodies.

(B) Cytoplasmic lysates of MCF7 cells transfected with control oligo, antagomiR-125b, TRIM21 siRNA, or antagomiR-125b and TRIM21 siRNA and exposed to UV irradiation were collected at designated time points post UV exposure and immunoblotted with HuR and GAPDH antibodies (left panels). Similarly treated cell lysates were also immunoblotted with p53 and GAPDH antibodies (right panels).

(C) Plots representing HuR and p53 band intensities from three independent experiments as described in (B) and corresponding best-fit curves. The band intensities of HuR and p53 were determined by densitometry and are normalized to corresponding GAPDH band intensities.

See also Figures S10 and S11.

lipopolysaccharide, and heat shock and regulates the stability or translation of multiple mRNAs (Ahuja et al., 2016; Gallouzi et al., 2001; Mazan-Mamczarz et al., 2003; Poria et al., 2016; Wang et al., 2000). The enhancement of p53 protein synthesis mediated by HuR appears to be crucial in attaining an increased steady-state level of p53, together with the stabilization of p53 protein by inhibition of its interaction with Mdm2. HuR increases p53 protein synthesis not only by directly enhancing p53 mRNA translation but also by preventing the repression of p53 translation by the UV-induced miRNA, miR-125b (Ahuja et al., 2016). The biphasic expression of miR-125b in response to UV allows an enhancement of p53 expression at early time points after UV exposure, but causes repression of p53 mRNA translation at later time points, thereby contributing to the pulsatile nature of p53 expression (Ahuja et al., 2016).

Such complex regulatory networks being amenable to computational modeling, we adopted an approach combining dynamic systems modeling with experimental validation to both understand the systems-level functioning of the p53 regulatory network and find novel regulatory components and interactions that may regulate p53 protein synthesis in response to UV-induced DNA damage. Failure of the network model to match with the experimental data might be due to errors in estimating the parameters used in simulating the model or might indicate the presence of hitherto unknown components or interactions in the network. Parametrization tests, by varying the parameters over a broad range of values, have indicated the absence of major deviations in estimating the parameters used for numerical simulation of the model (Figures S12–S15). Therefore the possibility of involvement of novel regulators of p53 expression was systematically investigated. The dynamics of p53 expression post DNA damage has been the subject of extensive investigation, both experimentally and computationally (Batchelor et al., 2008; Ciliberto et al., 2005; Geva-Zatorsky et al., 2006; Lahav et al., 2004; Lev Bar-Or et al., 2000; Zhang et al., 2007). The dynamics of p53 has been shown to vary substantially across cell lines and in response to different types of DNA-damaging stimuli (Batchelor et al., 2011; Stewart-Ornstein and Lahav, 2017). In our study in MCF7 cells, p53 showed a single broad pulse in response to non-ionizing UV radiation, as observed previously (Batchelor et al., 2011). We have investigated the role of the p53 mRNA translation regulatory network, specifically the translation regulators HuR and miR-125b, in generating this pulsatile change in p53 abundance in response to UV radiation. Among the few known regulators of HuR, miRNAs such as miR-519, miR-16, and miR-34a are reported to downregulate HuR levels (Abdelmohsen et al., 2010; Kojima et al., 2010; Xu et al., 2010). miR-192 has been shown to mediate positive feedback loops that regulate p53 oscillations in response to DNA double-strand breaks (Moore et al., 2015). miR-125a, a member of the miR-125 family, has been shown to be an inhibitor of HuR expression in breast cancer cells, although the same study found that miR-125b, another miR-125 family member, was much less effective in repressing HuR synthesis (Guo et al., 2009). Very recently, miR-125b has been shown to regulate HuR expression in hepatitis C virus-infected liver carcinoma cells (Shwetha et al., 2018). Our computational modeling and experimental observations have demonstrated miR-125b as a negative regulator of HuR protein synthesis in response to DNA damage. miR-125b has been found to target multiple genes in the p53 regulatory network, which includes regulators of both cell proliferation and apoptosis (Le et al., 2011). The demonstration of miR-125b as a regulator of HuR, together with its direct regulation of p53 mRNA translation, establishes it as a major player in the regulation of p53 expression.

The decrease in HuR and p53 levels in the later time period post UV exposure is partially due to translation repression by miR-125b. However, as inclusion of miR-125b as a repressor of HuR protein synthesis failed to generate the pulsatile behavior of HuR and p53, we considered degradation of HuR protein contributing to oscillatory behavior of p53. Despite its stability, HuR protein destabilization by ubiquitin-mediated proteolysis or caspase-mediated cleavage is observed in response to stresses such as moderate heat shock, glycolysis inhibition, DNA damage, and $CoCl_2$-induced hypoxia (Abdelmohsen et al., 2009; Chu et al.,

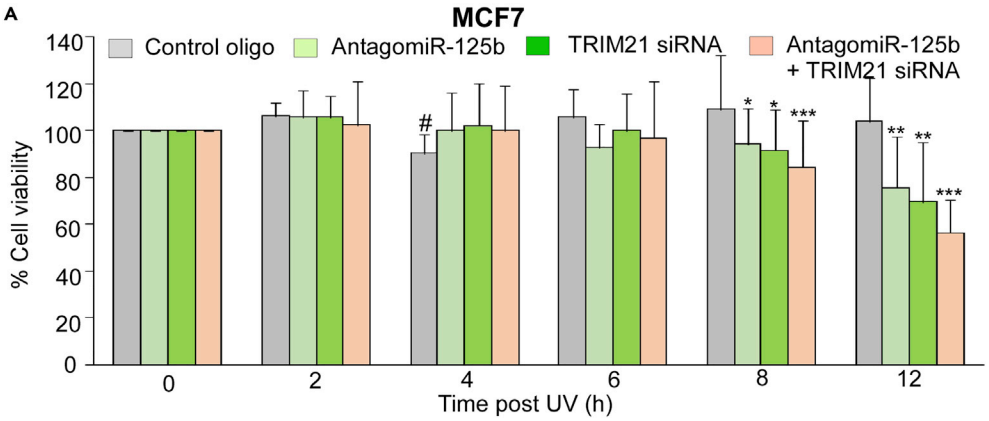
A
MCF7
Control oligo
AntagomiR-125b
TRIM21 siRNA
AntagomiR-125b + TRIM21 siRNA
% Cell viability
Time post UV (h)

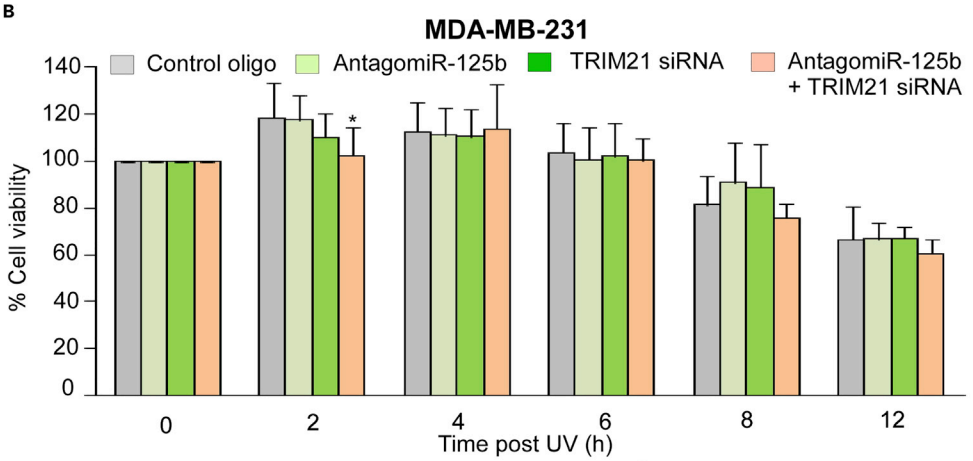
B
MDA-MB-231
Control oligo
AntagomiR-125b
TRIM21 siRNA
AntagomiR-125b + TRIM21 siRNA
% Cell viability
Time post UV (h)

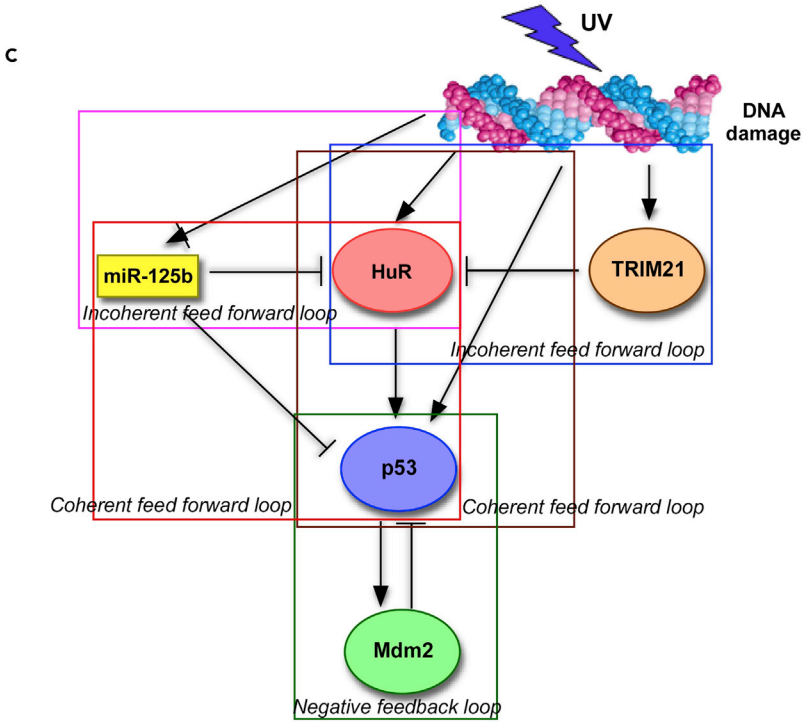
C
UV
DNA damage
miR-125b
HuR
TRIM21
Incoherent feed forward loop
Incoherent feed forward loop
p53
Coherent feed forward loop
Coherent feed forward loop
Mdm2
Negative feedback loop

Figure 7. The p53 Translation Regulation Network Regulates Cell Viability in Response to UV-Induced DNA Damage

(A) MTT (3-(4,5-dimethylthiazol-2-yl)-2,5-diphenyltetrazolium bromide) assay of MCF7 cells transfected with control oligo, antagomiR-125b, TRIM21 siRNA, and both antagomiR-125b and TRIM21 siRNA and collected at designated time points post UV irradiation. *$p \leq 0.05$, **$p \leq 0.01$, ***$p \leq 0.005$ of difference of cell viability from corresponding control oligo-transfected cells at the same time point. #$p \leq 0.05$ of difference of cell viability between control oligo-transfected cells between 0- and 4-h time points.

(B) MTT assay of MDA-MB-231 cells transfected with control oligo, antagomiR-125b, TRIM21 siRNA, and both antagomiR-125b and TRIM21 siRNA and collected at designated time points post UV irradiation. *$p \leq 0.05$ of difference from corresponding control oligo-transfected cells at the same time point.

(C) Network diagram representing the regulation of p53 mediated by HuR, miR-125b, TRIM21, and Mdm2 in response to UV-induced DNA damage. The network consists of overlapping incoherent and coherent feedforward loops and negative feedback loop with HuR and p53 as the central axis.

See also Figure S16.

2012; Lucchesi et al., 2016; Talwar et al., 2011). Postulating an unknown factor as mediating the degradation of HuR in response to UV, we found the E3 ubiquitin ligase TRIM21 to be responsible for ubiquitinating HuR leading to its proteasomal degradation. TRIM21, a 52-kD ribonucleoprotein, also denoted as Ro-SSA, is an autoantigen in autoimmune diseases such as systemic lupus erythematosus, rheumatoid arthritis, and Sjögren's syndrome (Ben-Chetrit et al., 1990). TRIM21 functions as a cytosolic IgG receptor known to bind the antibody Fc region via its C-terminal PRYSPRY domain and as an E3 ubiquitin ligase via its N-terminal RING domain (Ikeda and Inoue, 2012; James et al., 2007). TRIM21 negatively regulates the innate immune response to intracellular double-stranded DNA and DNA viruses by ubiquitinating DDX41 and targeting it for degradation (Zhang et al., 2012). It is also an important player in limiting the interferon response by targeting IRF3, IRF5, and other interferon response factors for proteasomal degradation (Higgs et al., 2008; Lazzari et al., 2014). Observations from TRIM21 knockout mice suggest that TRIM21 is a negative regulator of proinflammatory cytokine production and interferon signaling (Espinosa et al., 2009; Yoshimi et al., 2009). TRIM21 is also reported to reduce cell proliferation and acts as a pro-apoptotic molecule by suppressing Bcl-2 expression (Espinosa et al., 2006; Jauharoh et al., 2012). Therefore TRIM21 might play an important role as a link in limiting the inflammatory response and suppressing tumorigenesis. TRIM21 has been connected to regulation of p53 by its role in ubiquitinating guanosine 5′-monophosphate synthase and causing its nuclear localization, which contributes to dissociation of p53 from Mdm2 and its stabilization (Reddy et al., 2014). Our observations now demonstrate a new role for TRIM21 in fine-tuning p53 protein synthesis by modulating HuR protein level in response to UV radiation. This adds a new layer of regulation in the p53 control network activated by DNA damage.

Together, these observations have provided the basis of a systematic approach consisting of computational modeling and biochemical experimentation, which has allowed further elucidation of the intricate regulatory network controlling p53 expression and cell behavior in response to genotoxic stress. The translation regulatory network of p53 in response to UV-induced DNA damage consists of two overlapping incoherent feedforward loops (I-FFL) and two overlapping coherent feedforward loops (C-FFL) with HuR-p53 as the central axis (Figure 7C). Type1 I-FFLs function as pulse generators and response time accelerators, whereas C-FFLs constitute sign-sensitive delay elements that act as persistence detectors, which cause changes in gene expression only in response to persistent signals and protect against brief input fluctuations (Mangan and Alon, 2003). The type 1 I-FFLs in the p53 regulatory network involve damaged DNA, miR-125b, and TRIM21, which act in combination to generate a pulse of HuR (Figure S16). This pulse of HuR, combined with the pulse of miR-125b, which is opposite in phase, allows p53 mRNA translation to oscillate in response to DNA damage. The C-FFLs in the p53 regulatory network include a type 1 C-FFL, which involves damaged DNA, HuR, and p53, and a type 2 C-FFL consisting of miR-125b, HuR, and p53 (Figure S16). These two C-FFLs act in concert to enhance cellular p53 level only in response to persistent DNA damage. The integration of these incoherent and coherent feedforward loops with the p53-Mdm2 negative feedback loops causes the pulsatile change in p53 level in response to genotoxic stress and gives a window of opportunity to the cells to re-enter the cell cycle and resume cell division.

Limitations of the Study

This study develops and validates a mathematical model for the regulation of p53 expression in response to DNA damage that includes the regulators of p53 protein synthesis and stabilization. However, the model excludes the dynamics of the upstream regulators of p53 activation, such as the sensor and effector kinases

(Maréchal and Zou, 2013), assuming these to be reflected in the dynamics of Mdm2, their downstream target. The proposed mathematical model can be said to capture the major contributing factors of the modeled phenomena if the model results are close to the experimental observations. However, it is a partial model, and the regulatory system, owing to its high level of complexity, will have aspects that are unaccounted for in the model (Aris and Penn, 1980). Explicit inclusion of the dynamics of the upstream regulators of p53 activation would lead to further refinement of the model and may lead to the discovery of other novel regulators and mediators of the cellular DNA damage response.

METHODS

All methods can be found in the accompanying Transparent Methods supplemental file.

SUPPLEMENTAL INFORMATION

Supplemental Information can be found online at https://doi.org/10.1016/j.isci.2019.05.002.

ACKNOWLEDGMENTS

We thank S. Das (IISc. Bangalore, India), S. N. Bhattacharyya (CSIR-IICB, Kolkata, India), and S. K. Singh (BHU, Varanasi, India) for providing reagents and Paul L. Fox (LRI, Cleveland Clinic, Cleveland, USA) for providing laboratory facilities. This work was supported by a Wellcome Trust-DBT India Alliance intermediate fellowship (WT500139/Z/09/Z) to P.S.R., UGC senior research fellowship to D.A., IISER Kolkata senior research fellowship to A. Guha, and CSIR senior research fellowship to S.D.M. The Orbitrap Elite instrument (Proteomics and Metabolomics Core, LRI, Cleveland Clinic) was purchased via an NIH shared instrument grant, 1S10RR031537-01.

AUTHOR CONTRIBUTIONS

Conceptualization, P.S.R. and B.P.; Methodology, P.S.R., B.P., S.D.M., and A. Ghosh; Investigation, A. Guha, D.A., B.P., S.D.M., K.D., and B.W.; Resources, D.R. and V.S., Writing, P.S.R., A. Guha, and S.D.M.; Supervision, P.S.R.; Funding Acquisition, P.S.R.

DECLARATION OF INTERESTS

The authors declare no competing interests.

Received: September 25, 2018
Revised: December 20, 2018
Accepted: May 1, 2019
Published: May 31, 2019

REFERENCES

Abdelmohsen, K., Srikantan, S., Yang, X., Lal, A., Kim, H.H., Kuwano, Y., Galban, S., Becker, K.G., Kamara, D., de Cabo, R., et al. (2009). Ubiquitin-mediated proteolysis of HuR by heat shock. EMBO J. *28*, 1271–1282.

Abdelmohsen, K., Kim, M.M., Srikantan, S., Mercken, E.M., Brennan, S.E., Wilson, G.M., de Cabo, R., and Gorospe, M. (2010). miR-519 suppresses tumor growth by reducing HuR levels. Cell Cycle *9*, 1354–1359.

Ahuja, D., Goyal, A., and Ray, P.S. (2016). Interplay between RNA-binding protein HuR and microRNA-125b regulates p53 mRNA translation in response to genotoxic stress. RNA Biol. *13*, 1152–1165.

Aris, R., and Penn, M. (1980). The mere notion of a model. Math. Model. *1*, 1–12.

Batchelor, E., Mock, C.S., Bhan, I., Loewer, A., and Lahav, G. (2008). Recurrent initiation: a mechanism for triggering p53 pulses in response to DNA damage. Mol. Cell *30*, 277–289.

Batchelor, E., Loewer, A., Mock, C., and Lahav, G. (2011). Stimulus-dependent dynamics of p53 in single cells. Mol. Syst. Biol. *7*, 1–8.

Ben-Chetrit, E., Fox, R.I., and Tan, E.M. (1990). Dissociation of immune responses to the SS-A (Ro) 52-kd and 60-kd polypeptides in systemic lupus erythematosus and Sjögren's syndrome. Arthritis Rheum. *33*, 349–355.

Chu, P.-C., Chuang, H.-C., Kulp, S.K., and Chen, C.-S. (2012). The mRNA-stabilizing factor HuR protein is targeted by β-TrCP protein for degradation in response to glycolysis inhibition. J. Biol. Chem. *287*, 43639–43650.

Ciliberto, A., Novak, B., and Tyson, J.J. (2005). Steady states and oscillations in the p53/Mdm2 network. Cell Cycle *4*, 488–493.

Collister, M., Lane, D.P., and Kuehl, B.L. (1998). Differential expression of p53, p21(waf1/cip1) and hdm2 dependent on DNA damage in Bloom's syndrome fibroblasts. Carcinogenesis *19*, 2115–2120.

Espinosa, A., Zhou, W., Ek, M., Hedlund, M., Brauner, S., Popovic, K., Horvath, L., Wallerskog, T., Oukka, M., Nyberg, F., et al. (2006). The Sjogren's syndrome-associated autoantigen Ro52 is an E3 ligase that regulates proliferation and cell death. J. Immunol. *176*, 6277–6285.

Espinosa, A., Dardalhon, V., Brauner, S., Ambrosi, A., Higgs, R., Quintana, F.J., Sjöstrand, M., Eloranta, M.-L., Ní Gabhann, J., Winqvist, O., et al. (2009). Loss of the lupus autoantigen Ro52/Trim21 induces tissue inflammation and systemic autoimmunity by disregulating the IL-23-Th17 pathway. J. Exp. Med. *206*, 1661–1671.

Fu, L., Minden, M.D., and Benchimol, S. (1996). Translational regulation of human p53 gene expression. EMBO J. *15*, 4392–4401.

Gaglia, G., and Lahav, G. (2014). Constant rate of p53 tetramerization in response to DNA damage controls the p53 response. Mol. Syst. Biol. *10*, 1–8.

Gallouzi, I.E., Brennan, C.M., and Steitz, J.A. (2001). Protein ligands mediate the CRM1-dependent export of HuR in response to heat shock. RNA *7*, 1348–1361.

Geva-Zatorsky, N., Rosenfeld, N., Itzkovitz, S., Milo, R., Sigal, A., Dekel, E., Yarnitzky, T., Liron, Y., Polak, P., Lahav, G., et al. (2006). Oscillations and variability in the p53 system. Mol. Syst. Biol. *2*, 1–13.

Guo, X., Wu, Y., and Hartley, R.S. (2009). MicroRNA-125a represses cell growth by targeting HuR in breast cancer. RNA Biol. *6*, 575–583.

Higgs, R., Ní Gabhann, J., Ben Larbi, N., Breen, E.P., Fitzgerald, K.A., and Jefferies, C.A. (2008). The E3 ubiquitin ligase Ro52 negatively regulates IFN-beta production post-pathogen recognition by polyubiquitin-mediated degradation of IRF3. J. Immunol. *181*, 1780–1786.

Horn, H.F., and Vousden, K.H. (2007). Coping with stress: multiple ways to activate p53. Oncogene *26*, 1306–1316.

Ikeda, K., and Inoue, S. (2012). TRIM proteins as RING finger E3 ubiquitin ligases. Adv. Exp. Med. Biol. *770*, 27–37.

James, L.C., Keeble, A.H., Khan, Z., Rhodes, D.A., and Trowsdale, J. (2007). Structural basis for PRYSPRY-mediated tripartite motif (TRIM) protein function. Proc. Natl. Acad. Sci. U S A *104*, 6200–6205.

Jauharoh, S.N.A., Saegusa, J., Sugimoto, T., Ardianto, B., Kasagi, S., Sugiyama, D., Kurimoto, C., Tokuno, O., Nakamachi, Y., Kumagai, S., et al. (2012). SS-A/Ro52 promotes apoptosis by regulating Bcl-2 production. Biochem. Biophys. Res. Commun. *417*, 582–587.

Kastan, M.B., Onyekwere, O., Sidransky, D., Vogelstein, B., and Craig, R.W. (1991). Participation of p53 protein in the cellular response to DNA damage. Cancer Res. *51*, 6304–6311.

Kojima, K., Fujita, Y., Nozawa, Y., Deguchi, T., and Ito, M. (2010). MiR-34a attenuates paclitaxel-resistance of hormone-refractory prostate cancer PC3 cells through direct and indirect mechanisms. Prostate *70*, 1501–1512.

Lahav, G. (2008). Oscillations by the p53-Mdm2 feedback loop. Adv. Exp. Med. Biol. *641*, 28–38.

Lahav, G., Rosenfeld, N., Sigal, A., Geva-Zatorsky, N., Levine, A.J., Elowitz, M.B., and Alon, U. (2004). Dynamics of the p53-Mdm2 feedback loop in individual cells. Nat. Genet. *36*, 147–150.

Lazzari, E., Korczeniewska, J., Ní Gabhann, J., Smith, S., Barnes, B.J., and Jefferies, C.A. (2014). TRIpartite motif 21 (TRIM21) differentially regulates the stability of interferon regulatory factor 5 (IRF5) isoforms. PLoS One *9*, e103609.

Le, M.T.N., Teh, C., Shyh-Chang, N., Xie, H., Zhou, B., Korzh, V., Lodish, H.F., and Lim, B. (2009). MicroRNA-125b is a novel negative regulator of p53. Genes Dev. *23*, 862–876.

Le, M.T.N., Shyh-Chang, N., Khaw, S.L., Chin, L., Teh, C., Tay, J., O'Day, E., Korzh, V., Yang, H., Lal, A., et al. (2011). Conserved regulation of p53 network dosage by microRNA-125b occurs through evolving miRNA-target gene pairs. PLoS Genet. *7*, e1002242.

Lev Bar-Or, R., Maya, R., Segel, L.A., Alon, U., Levine, A.J., and Oren, M. (2000). Generation of oscillations by the p53-Mdm2 feedback loop: a theoretical and experimental study. Proc. Natl. Acad. Sci. U S A *97*, 11250–11255.

Lucchesi, C., Sheikh, M.S., and Huang, Y. (2016). Negative regulation of RNA-binding protein HuR by tumor-suppressor ECRG2. Oncogene *35*, 2565–2573.

Ma, L., Wagner, J., Rice, J.J., Hu, W., Levine, A.J., and Stolovitzky, G.A. (2005). A plausible model for the digital response of p53 to DNA damage. Proc. Natl. Acad. Sci. U S A *102*, 14266–14271.

Mangan, S., and Alon, U. (2003). Structure and function of the feed-forward loop network motif. Proc. Natl. Acad. Sci. U S A *100*, 11980–11985.

Maréchal, A., and Zou, L. (2013). DNA damage sensing by the ATM and ATR kinases. Cold Spring Harb. Perspect. Biol. *5*, a012716.

Mazan-Mamczarz, K., Galbán, S., López de Silanes, I., Martindale, J.L., Atasoy, U., Keene, J.D., and Gorospe, M. (2003). RNA-binding protein HuR enhances p53 translation in response to ultraviolet light irradiation. Proc. Natl. Acad. Sci. U S A *100*, 8354–8359.

Michael, D., and Oren, M. (2003). The p53-Mdm2 module and the ubiquitin system. Semin. Cancer Biol. *13*, 49–58.

Moore, R., Ooi, H.K., Kang, T., Bleris, L., and Ma, L. (2015). MiR-192-Mediated positive feedback loop controls the robustness of stress-induced p53 oscillations in breast cancer cells. PLoS Comput. Biol. *11*, e1004653.

Poria, D.K., Guha, A., Nandi, I., and Ray, P.S. (2016). RNA-binding protein HuR sequesters microRNA-21 to prevent translation repression of proinflammatory tumor suppressor gene programmed cell death 4. Oncogene *35*, 1703–1715.

Proctor, C.J., and Gray, D.A. (2008). Explaining oscillations and variability in the p53-Mdm2 system. BMC Syst. Biol. *2*, 75.

Purvis, J.E., Karhohs, K.W., Mock, C., Batchelor, E., Loewer, A., and Lahav, G. (2012). p53 dynamics control cell fate. Science *336*, 1440–1444.

Reddy, B.A., van der Knaap, J.A., Bot, A.G.M., Mohd-Sarip, A., Dekkers, D.H.W., Timmermans, M.A., Martens, J.W.M., Demmers, J.A.A., and Verrijzer, C.P. (2014). Nucleotide biosynthetic enzyme GMP synthase is a TRIM21-controlled relay of p53 stabilization. Mol. Cell *53*, 458–470.

Shwetha, S., Sharma, G., Raheja, H., Goel, A., Aggarwal, R., and Das, S. (2018). Interaction of miR-125b-5p with Human antigen R mRNA: mechanism of controlling HCV replication. Virus Res. *258*, 1–8.

Stewart-Ornstein, J., and Lahav, G. (2017). P53 dynamics in response to DNA damage vary across cell lines and are shaped by efficiency of DNA repair and activity of the kinase ATM. Sci. Signal. *10*, eaah6671.

Talwar, S., Jin, J., Carroll, B., Liu, A., Gillespie, M.B., and Palanisamy, V. (2011). Caspase-mediated cleavage of RNA-binding protein HuR regulates c-Myc protein expression after hypoxic stress. J. Biol. Chem. *286*, 32333–32343.

Vilborg, A., Wilhelm, M.T., and Wiman, K.G. (2010). Regulation of tumor suppressor p53 at the RNA level. J. Mol. Med. (Berl) *88*, 645–652.

Wagner, J., Ma, L., Rice, J.J., Hu, W., Levine, A.J., and Stolovitzky, G.A. (2005). p53-Mdm2 loop controlled by a balance of its feedback strength and effective dampening using ATM and delayed feedback. Syst. Biol. (Stevenage) *152*, 109–118.

Wang, W., Furneaux, H., Cheng, H., Caldwell, M.C., Hutter, D., Liu, Y., Holbrook, N., and Gorospe, M. (2000). HuR regulates p21 mRNA stabilization by UV light. Mol. Cell. Biol. *20*, 760–769.

Xu, F., Zhang, X., Lei, Y., Liu, X., Liu, Z., Tong, T., and Wang, W. (2010). Loss of repression of HuR translation by miR-16 may be responsible for the elevation of HuR in human breast carcinoma. J. Cell. Biochem. *111*, 727–734.

Yoshimi, R., Chang, T.-H., Wang, H., Atsumi, T., Morse, H.C., Ozato, K., and Ozato, K. (2009). Gene disruption study reveals a nonredundant role for TRIM21/Ro52 in NF-kappaB-dependent cytokine expression in fibroblasts. J. Immunol. *182*, 7527–7538.

Zhang, T., Brazhnik, P., and Tyson, J.J. (2007). Exploring mechanisms of the DNA-damage response: p53 pulses and their possible relevance to apoptosis. Cell Cycle *6*, 85–94.

Zhang, Y., Gao, J.-S., Tang, X., Tucker, L.D., Quesenberry, P., Rigoutsos, I., and Ramratnam, B. (2009). MicroRNA 125a and its regulation of the p53 tumor suppressor gene. FEBS Lett. *583*, 3725–3730.

Zhang, Z., Bao, M., Lu, N., Weng, L., Yuan, B., and Liu, Y.-J. (2012). The E3 ubiquitin ligase TRIM21 negatively regulates the innate immune response to intracellular double-stranded DNA. Nat. Immunol. *14*, 172–178.

ISCI, Volume *15*

Supplemental Information

Integrated Regulation of HuR by Translation Repression and Protein Degradation Determines Pulsatile Expression of p53 Under DNA Damage

Abhishek Guha, Deepika Ahuja, Sukhen Das Mandal, Bibudha Parasar, Krishanu Deyasi, Debadrita Roy, Vasundhara Sharma, Belinda Willard, Anandamohan Ghosh, and Partho Sarothi Ray

Figure S1. Related to Figure 1

A

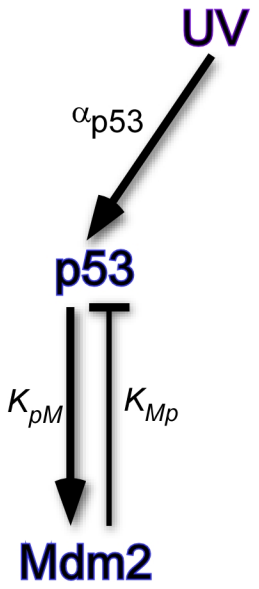

B

$$\frac{d[p53]}{dt} = \alpha_{p3} - K_{Mp}[Mdm2][p53] - \beta_{p53}[p53]$$

$$\frac{d[Mdm2]}{dt} = \alpha_{Mdm2}(1 + K_{pM}[p53]) - \beta_{Mdm2}[Mdm2]$$

C

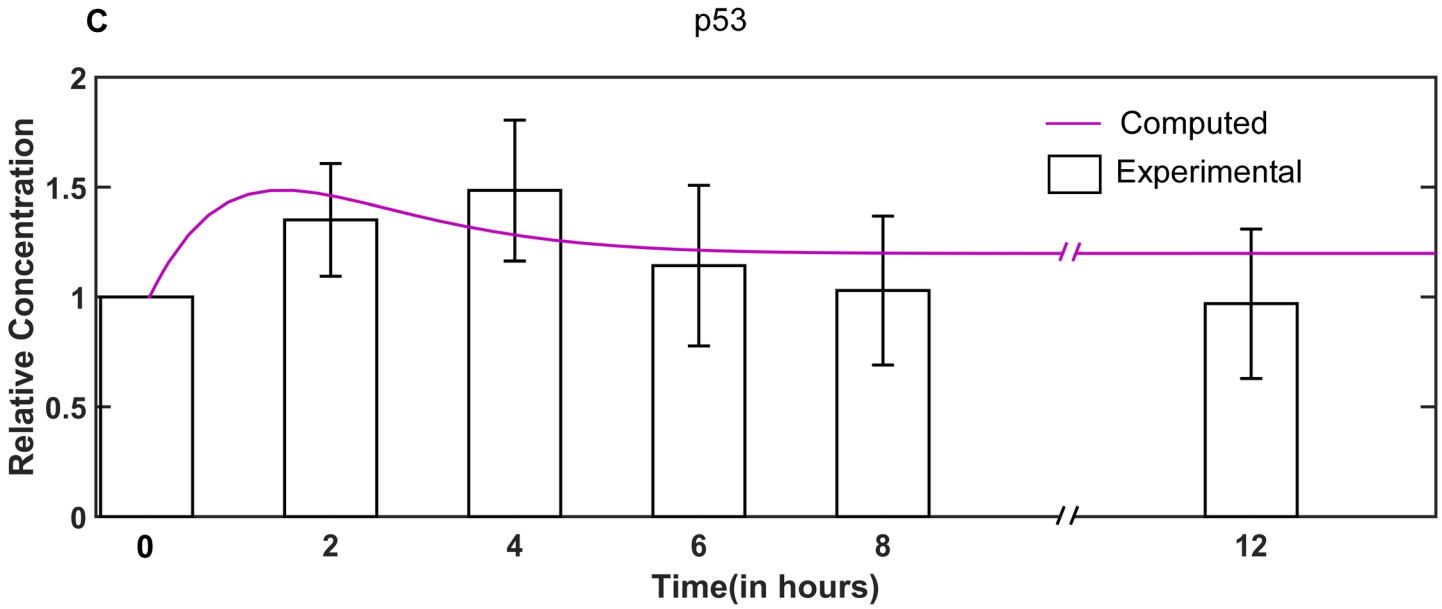

Modelling of the p53-Mdm2 negative feedback circuit shows a pulse of p53 in response to UV. (**A)** Network diagram of the minimal p53-Mdm2 negative feedback circuit in response to UV irradiation. (**B**) Rate equations representing the p53-Mdm2 negative feedback circuit in response to UV irradiation. (**C**) Plot representing simulation and bar graphs representing experimental data of change of p53 level over a 12 h period post-exposure to a 10 J/m^2 pulse of UVC irradiation. The simulation plot represents the numerical integration of the rate equations in (B). The bar graphs represent intensity values of p53 bands obtained from immunoblots of cell lysates collected at the designated time points post UV exposure, normalized to corresponding GAPDH band intensities . Data represents mean ± SD values from 7 independent immunoblots. The normalized band intensities are scaled to the 0 hour time point band intensity, taken as 1.

Figure S2. Related to Figure 2.

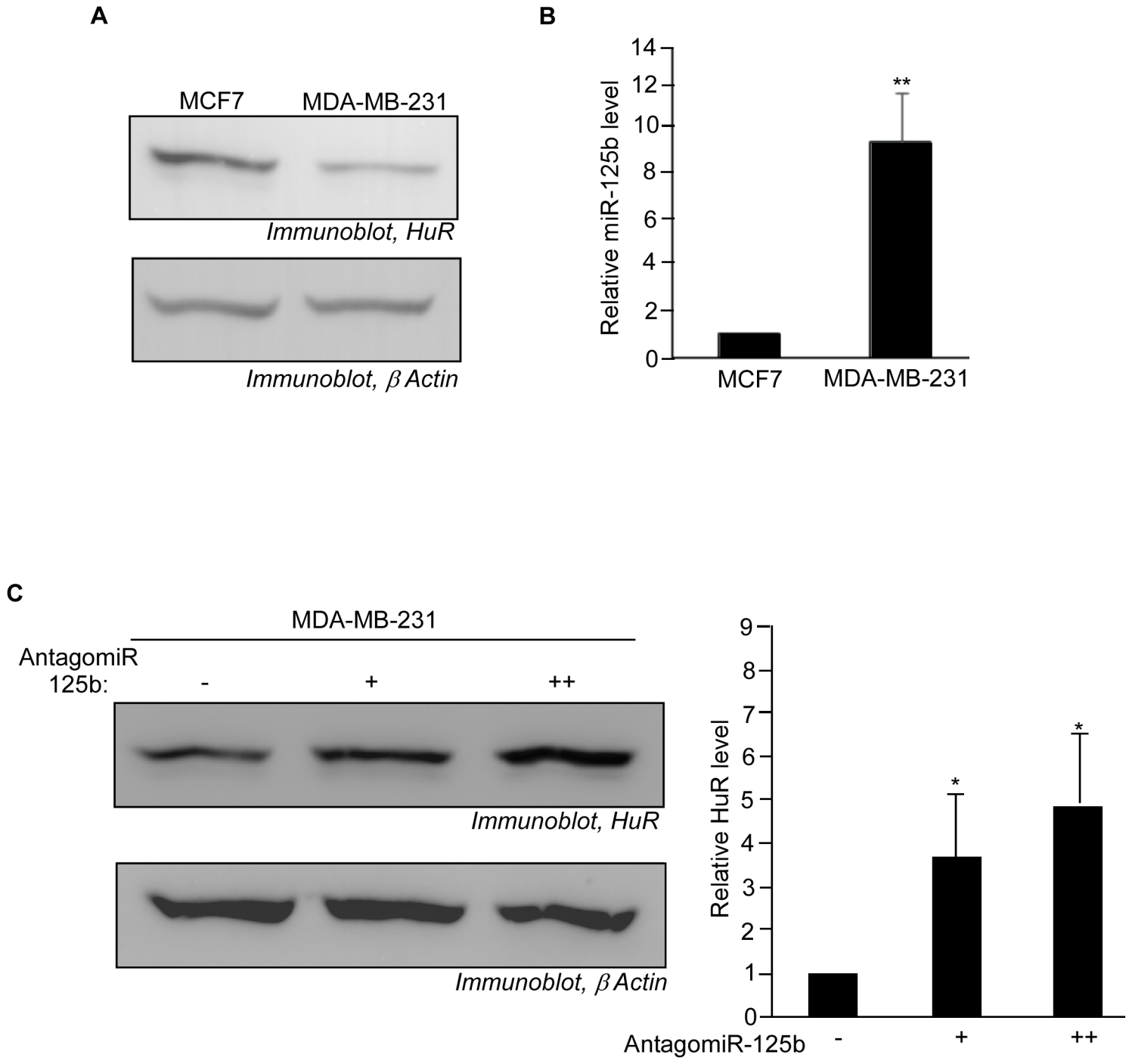

(A) Immunoblot of lysates from MCF7 and MDA-MB-231 cells with anti-HuR and anti- β-actin antibodies. (B) qRT-PCR of total RNA from MCF-7 and MDA-MB-231 with miR-125b specific primers. Data represents mean ± SD from two biological replicates, each with two technical replicates. (C) Immunoblot of lysates from MDA-MB-231 cells transfected with two increasing concentrations of antagomiR-125b with anti-HuR and anti- β-actin antibodies. * signifies a p-value </= 0.05 and ** signifies a p-value </= 0.01.

Figure S3. Related to Figure 2

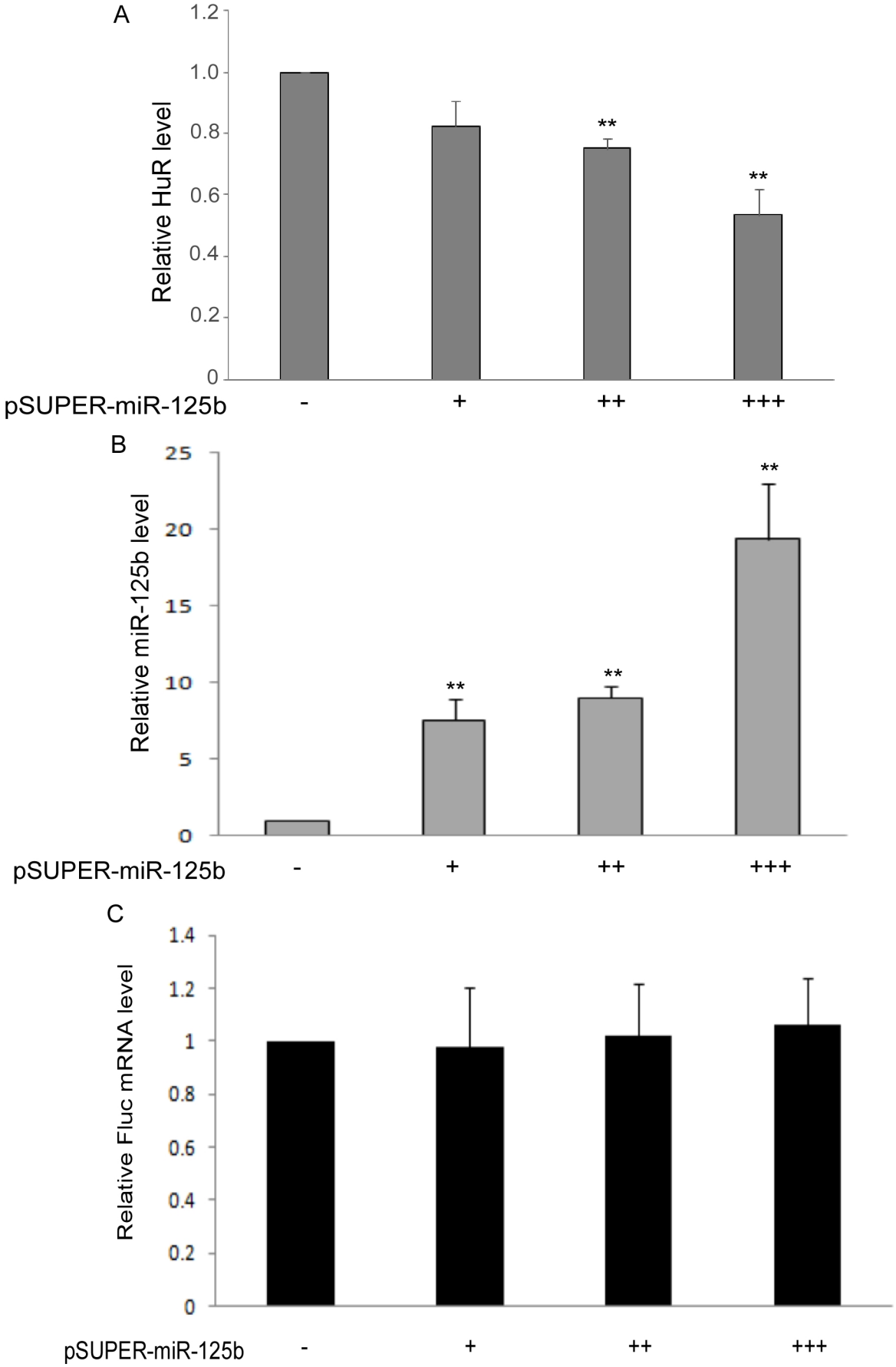

(A) Immunoblot of lysates from MCF-7 cells transfected with three increasng concentrations of miR-125b-expressing plasmid. HuR band intensities are normalized to corresponding GAPDH band intensities. (B) qRT-PCR of total RNA from MCF-7 cells cotransfected with three increasing concentrations of miR-125b-expressing plasmid and a plasmid containing HuR mRNA 3'UTR downstream of firefly luciferase gene with miR-125b specific primers. (C) qRT-PCR of total RNA from the same cells with firefly luciferase specific primers. Data represents mean ± SD from three independent experiments. ** signifies a p-value </= 0.01.

Figure S4. Related to Figure 2.

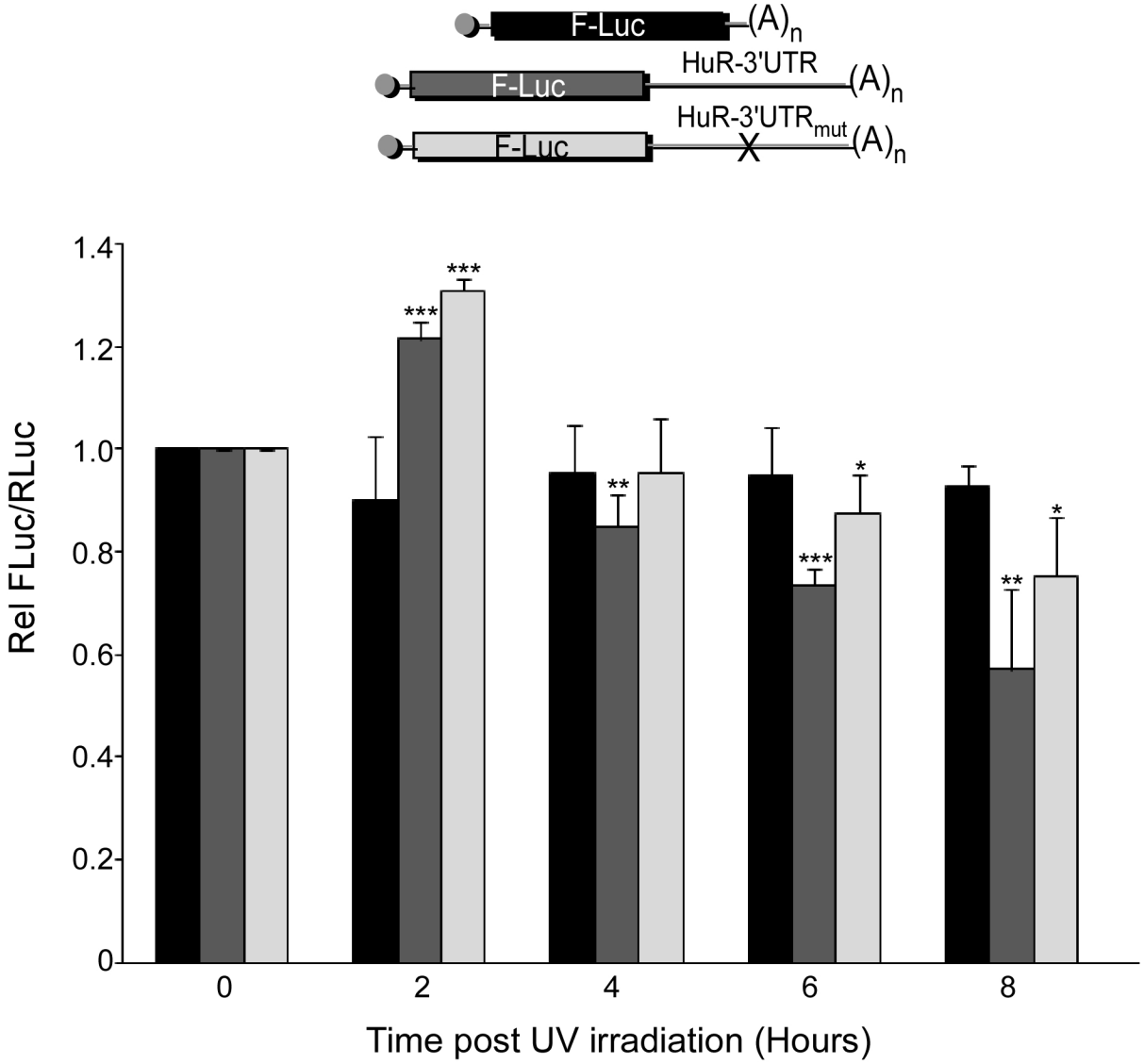

MCF-7 cells transfected with Firefly luciferase constructs without 3'UTR sequence or containing wild-type HuR mRNA 3'UTR or miR-125b binding site-mutated HuR mRNA 3'UTR was exposed to UV irradiation following which cells were collected at the designated time points and luciferase assay performed. Fluc values are normalized to Rluc values as transfection control. Data represents mean ± SD from three independent experiments each with two replicates. *signifies a p-value </= 0.05, ** signifies a p-value </= 0.01 and *** signifies a p-value </= 0.005.

Figure S5. Related to Figure 2

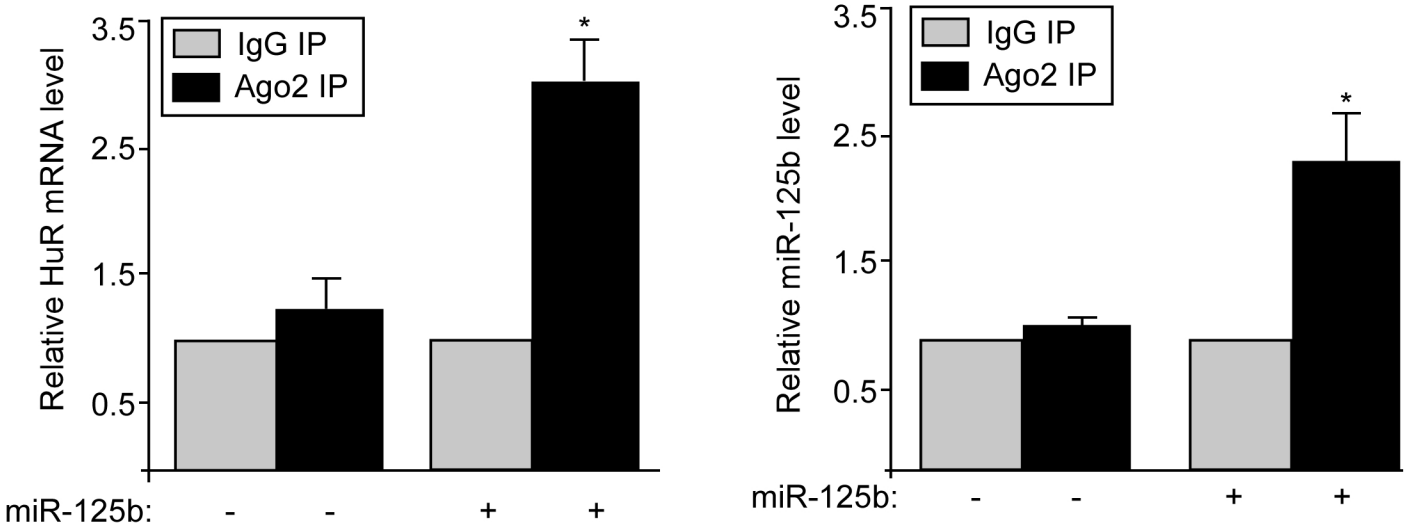

Lysates of MCF7 cells either mock transfected or transfected with miR-125b expressing construct were immunoprecipitated with anti-Ago2 anibody or non-immune IgG. RNA associated with the immunoprecipitates was isolated and associated HuR mRNA and miR-125b RNA levels were determined by qRT-PCR. Data represents mean ± SD from two biological replicates, each with two technical replicates. * signifies a p-value </= 0.05

Figure S6. Related to Figure 3

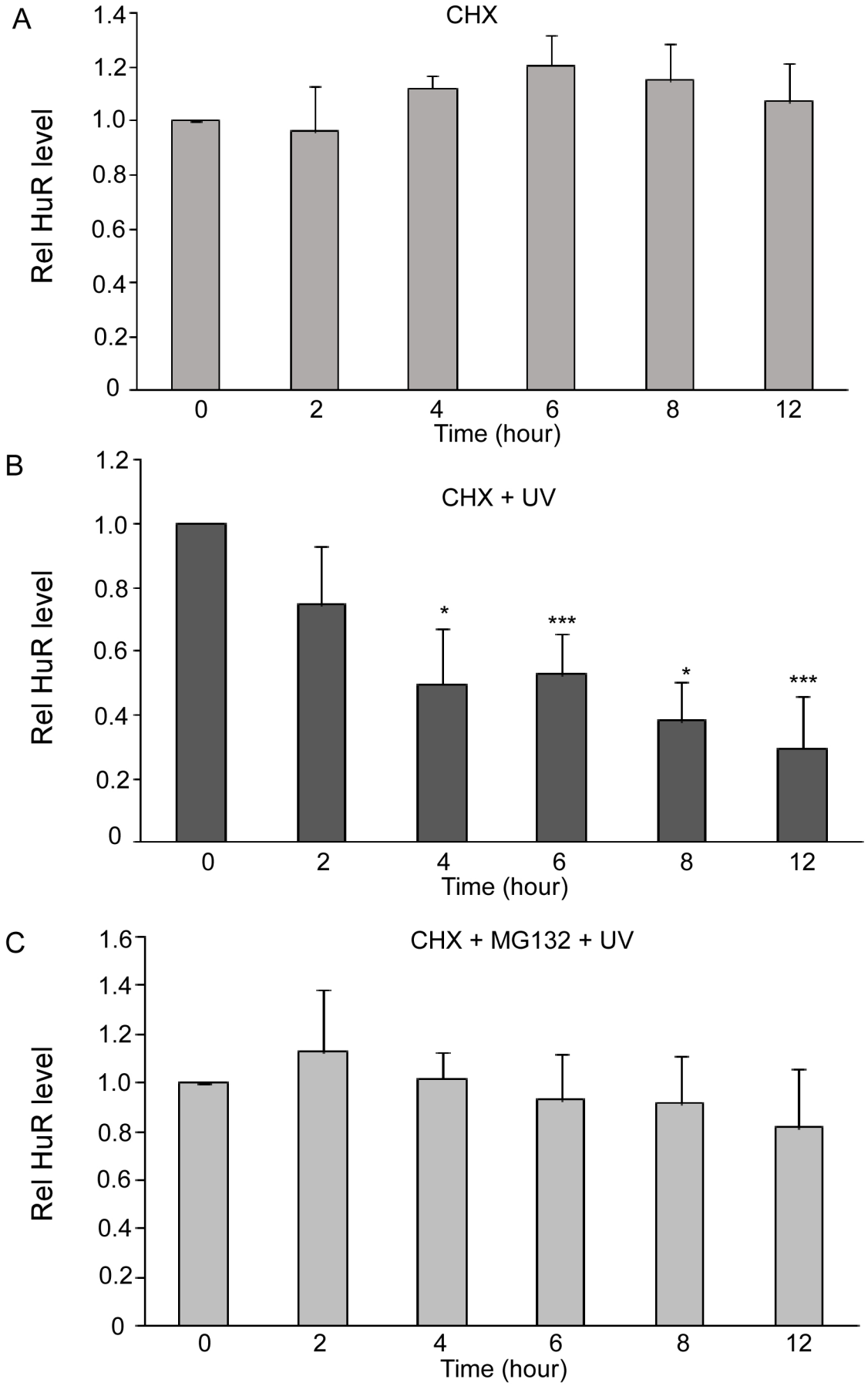

Immunoblots of lysates of MCF7 cells treated with cycloheximide (CHX) (A) or CHX and UV irradiation (B) and CHX and MG132 and UV irradiation (C) and collected at designated time points over a 12 hour period. Lysates were probed with HuR and GAPDH antibodies. HuR band intensities were normalized to GAPDH band intensities. Data represents mean ± SD from three independent experiments. * signifies a p-value </= 0.05, *** signifies p-value </= 0.005

Figure S7. Related to Figure 4

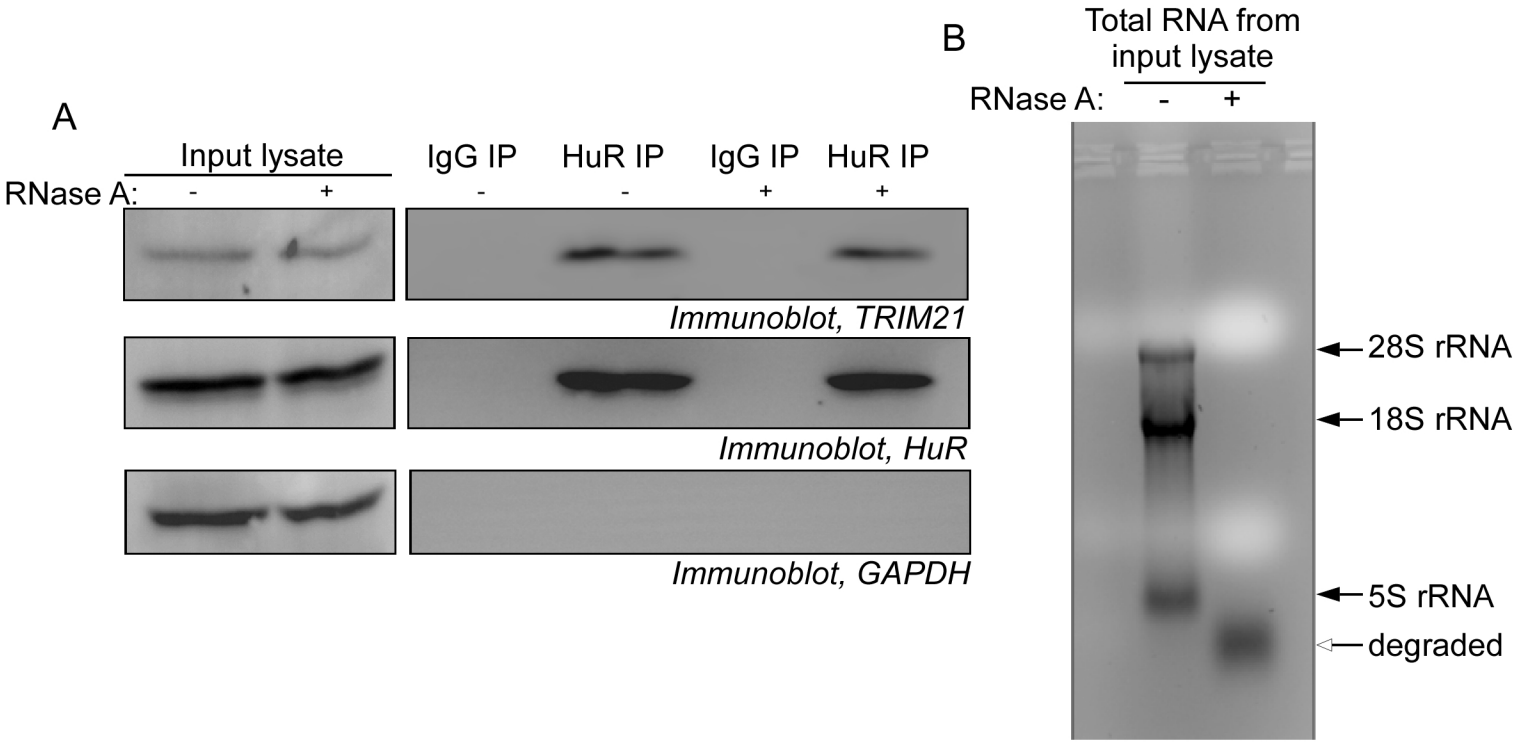

(A) Lysates of MCF7 cells were either treated or not treated with RNase A and immunoprecipitated with anti-HuR antibody or non-immune IgG. Immunoprecipitates and input lysates were immunoblotted with anti-TRIM21, HuR and GAPDH antibodies. (B) Total RNA isolated from input lysate without and with RNase A treatment was electrophoresed on agarore gel and stained with ethidium bromide.

Figure S8. Related to Figure 5.

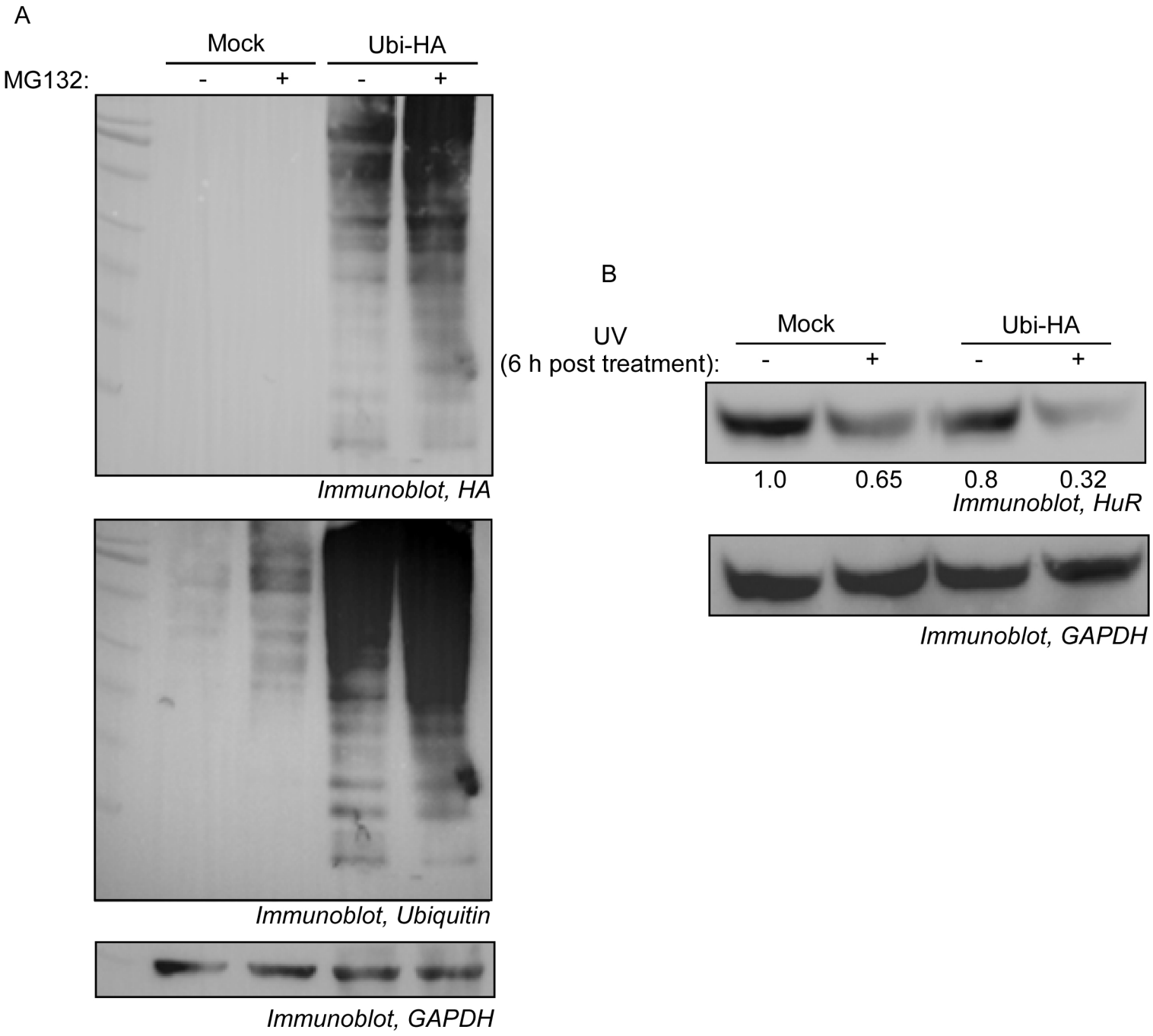

(A) Lysates of MCF7 cells either mock transfected of transfected with a construct expressing HA-tagged ubiquitin and treated with MG132 was immunoblotted with anti-HA and anti-ubiquitin antibodies. (B) MCF7 cells transfected as in (A) were collected 6 hours after UV irradiation and immunoblotted with anti-HuR and anti-GAPDH antibodies.

Figure S9. Related to Figure 5.

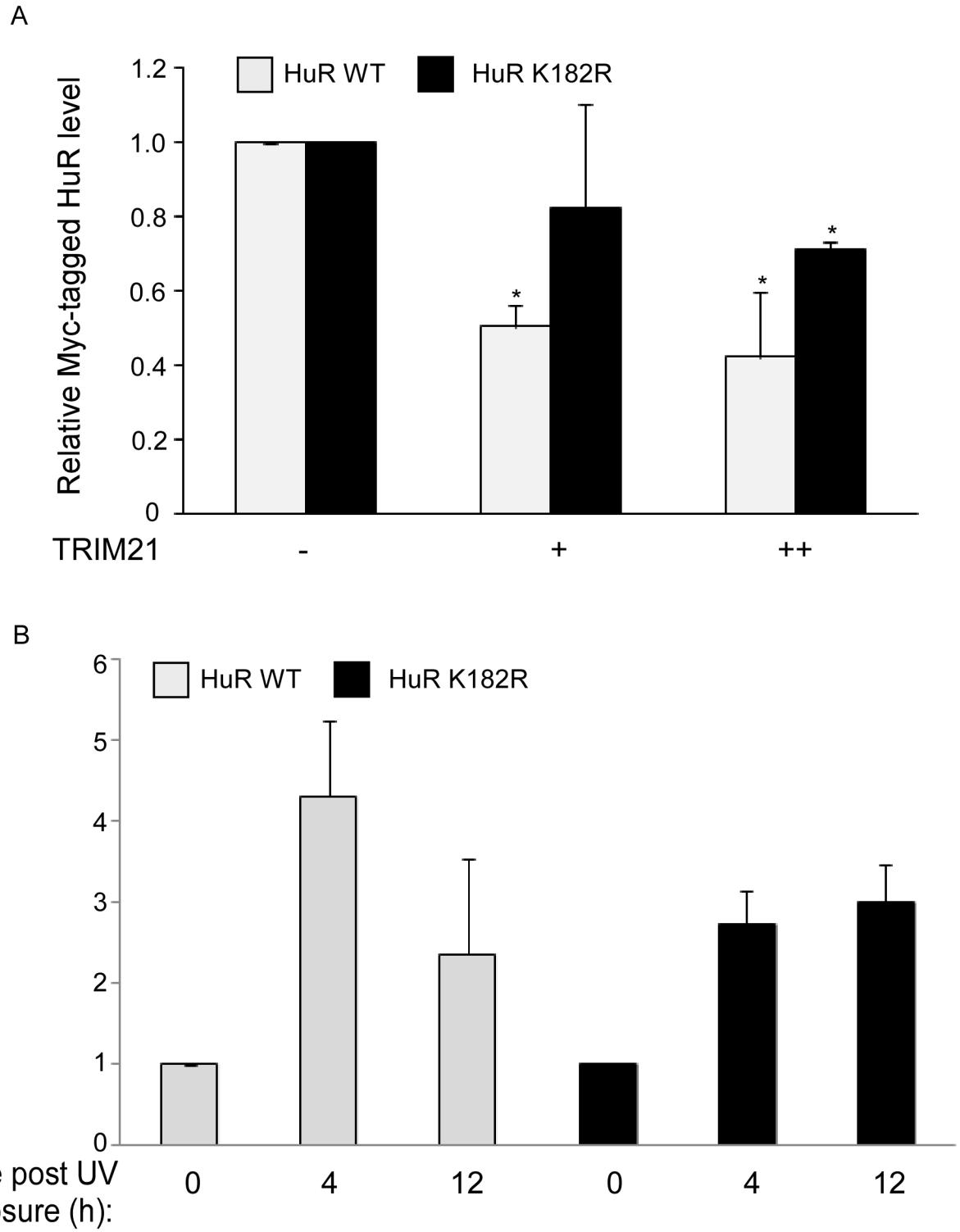

(A) Immunoblots of cell lysates expressing Myc-tagged HuR WT or HuR K182R transfected with three increasing concentrations of a construct expressing TRIM21. 48 hours post transfection cells were treated with CHX for 30 min and UV irradiated. Lysates were immunoblotted with anti-Myc and anti-β Actin antibodies. Myc-tagged HuR band intensities were normalized to β Actin band intensities. (B) Immunoblots of cytoplasmic lysates of cells expressing Myc-tagged HuR WT or HuR K182R and UV irradiated. Myc-tagged HuR band intensities were normalized to β Actin band intensities. Data represents mean ± SD from three independent experiments. * signifies a p-value </= 0.05.

Figure S10. Related to Figure 6.

A

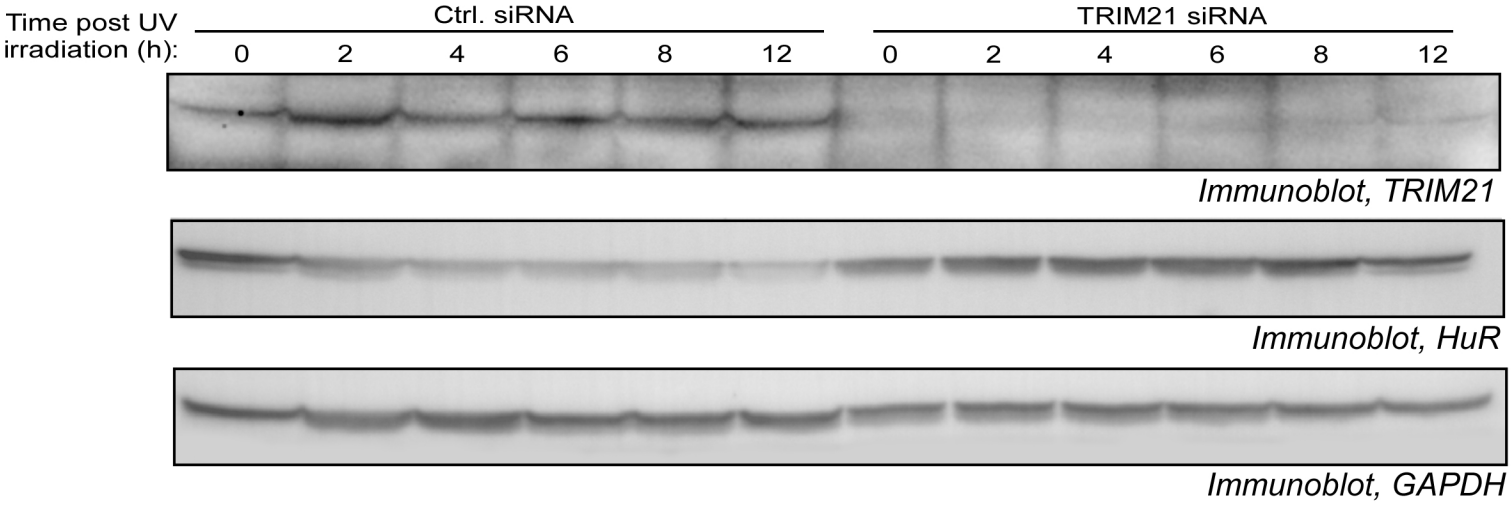

B

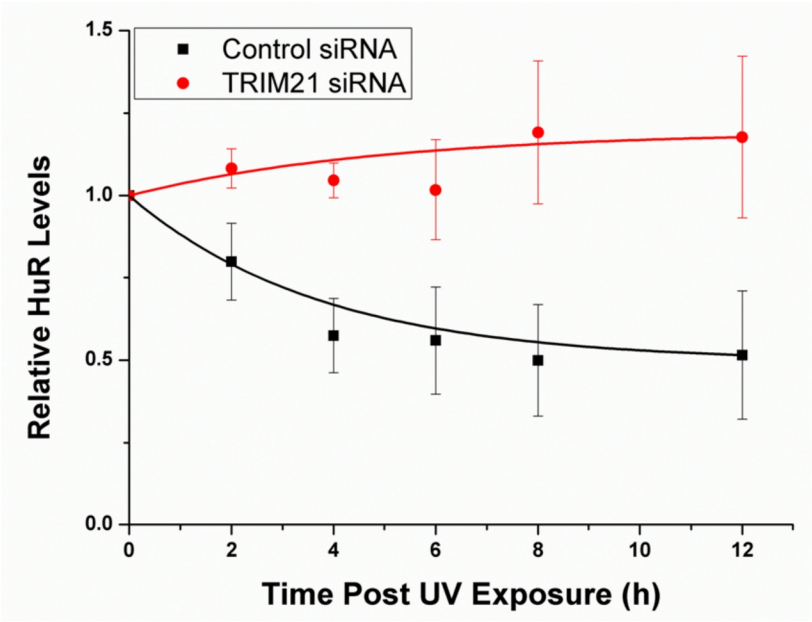

(A) Whole cell lysates of MCF7 cells transfected with control siRNA or TRIM21 siRNA and treated with CHX and collected at designated time points post exposure to 10 J/m^2 pulse of UV were immunoblotted with TRIM21, HuR and GAPDH antibodies.(B) Quantification of HuR levels, normalized to GAPDH, from three independent experiments showing Mean ± SD and best fit curves.

Figure S11. Related to Figure 6.

A

$$\frac{d[HuR]}{dt} = \alpha_{HuR} - K_{XH}[HuR][X] - \beta_{HuR}[HuR]$$

$$\frac{d[p53]}{dt} = \alpha_{p53}(1 + K_{Hp}[HuR]) - K_{Mp}[Mdm2][p53] - \beta_{p53}[p53]$$

$$\frac{d[Mdm2]}{dt} = \alpha_{Mdm2}(1 + K_{pM}[p53]) - \beta_{Mdm2}[Mdm2]$$

$$\frac{d[X]}{dt} = \alpha_X - \beta_X[X]$$

B

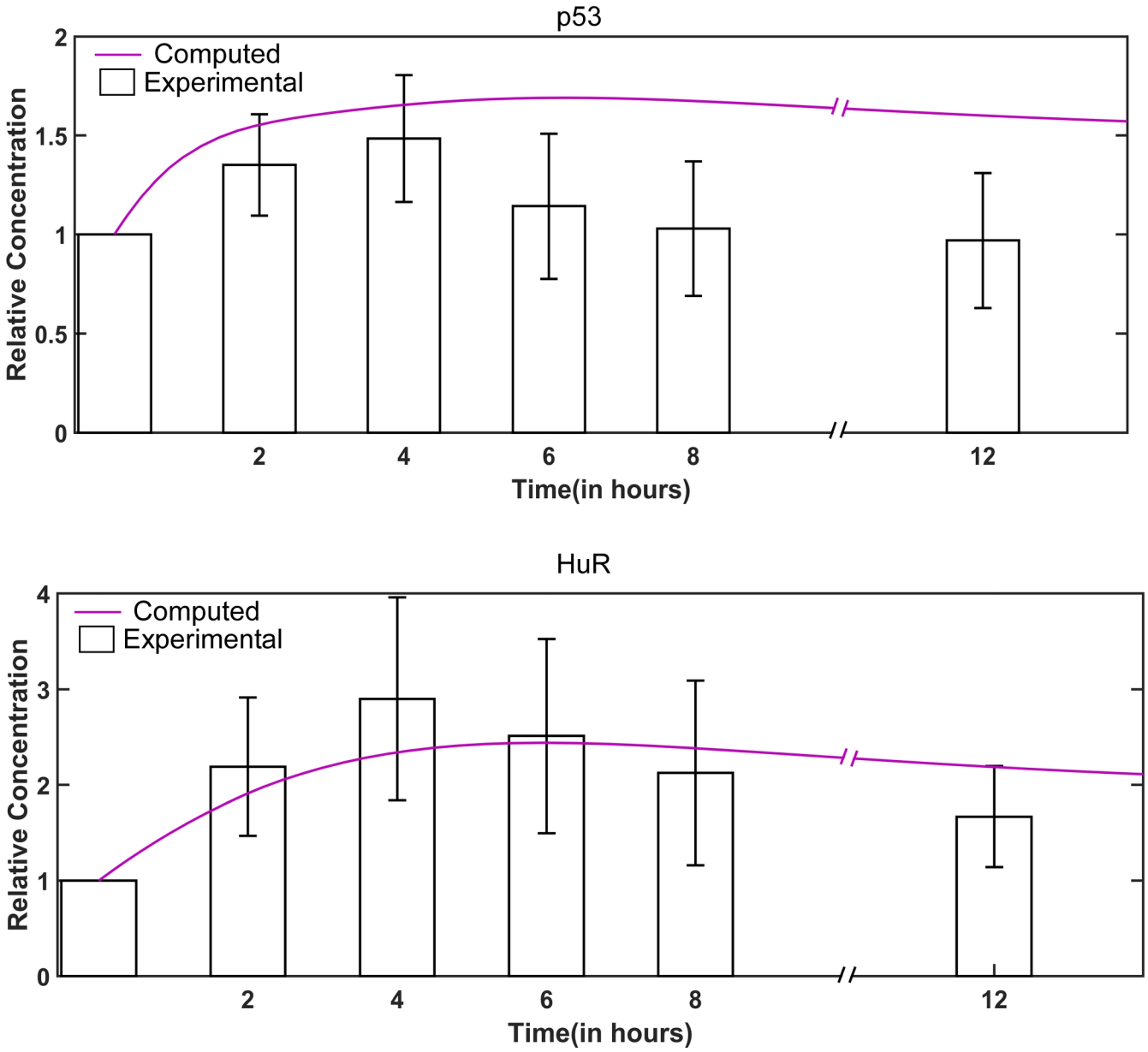

(A) Rate equations representing the p53 translation regulation network in response to UV irradiation. The rate equation for HuR expression contains a term representing the effect of X (K_{XH}) on HuR degradation. Terms representing the effect of miR-125b have been omitted from all equations. (B) Plots representing simulation and experimental data of change of p53 and HuR levels over a 12 hour period post exposure to a 10 J/m^2 pulse of UVC irradiation. The computed plots (purple lines) represent the numerical integration of the rate equations in (A). The experimental data is represented as bar graphs. Experimental data represents mean ± SD values from 7 independent immunoblots, normalized to corresponding GAPDH band intensities.

Figure S12. Related to Figure S1.

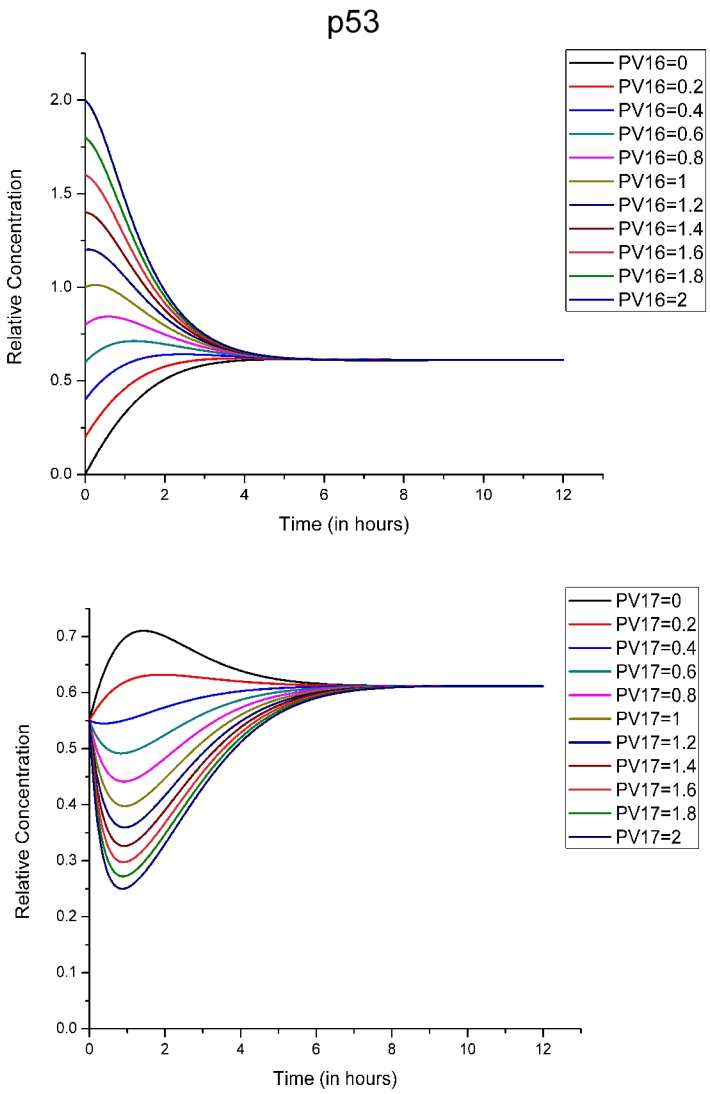

Estimation of robustness of Model 1 **(Figure S1)** by varying assumed parameters (initial conditions: p53 concentration (PV16) = 0.55 and Mdm2 concentration (PV17) = 0.05) between 0-2

Figure S13. Related to Figure 1.

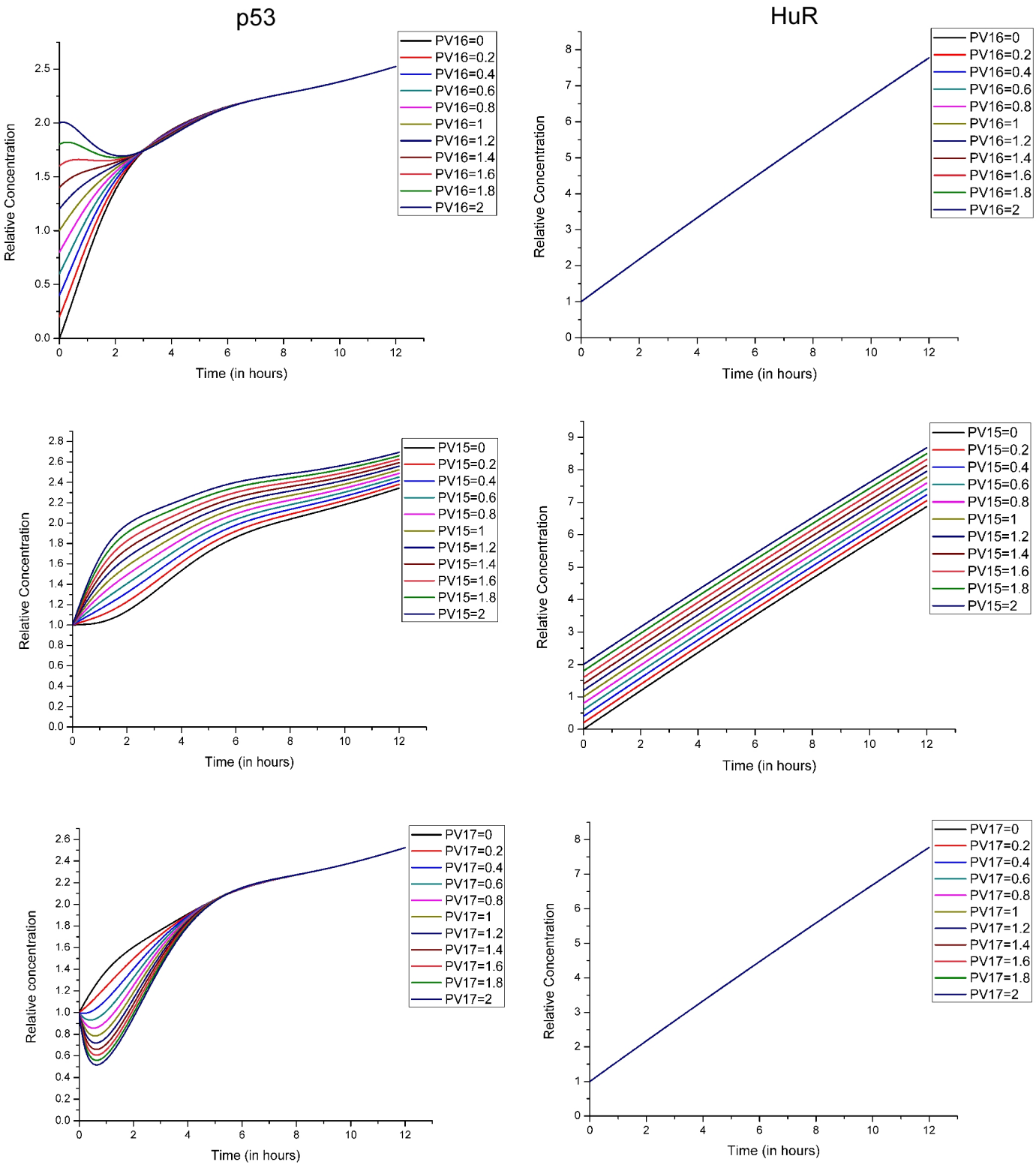

Estimation of robustness of Model 2 **(Figure 1B)** by varying assumed parameters (initial conditions: p53 concentration (PV16) = 1, HuR concentration (PV15) = 1, and Mdm2 concentration (PV17) = 0.05) between 0-2.

Figure S14. Related to Figure 2.

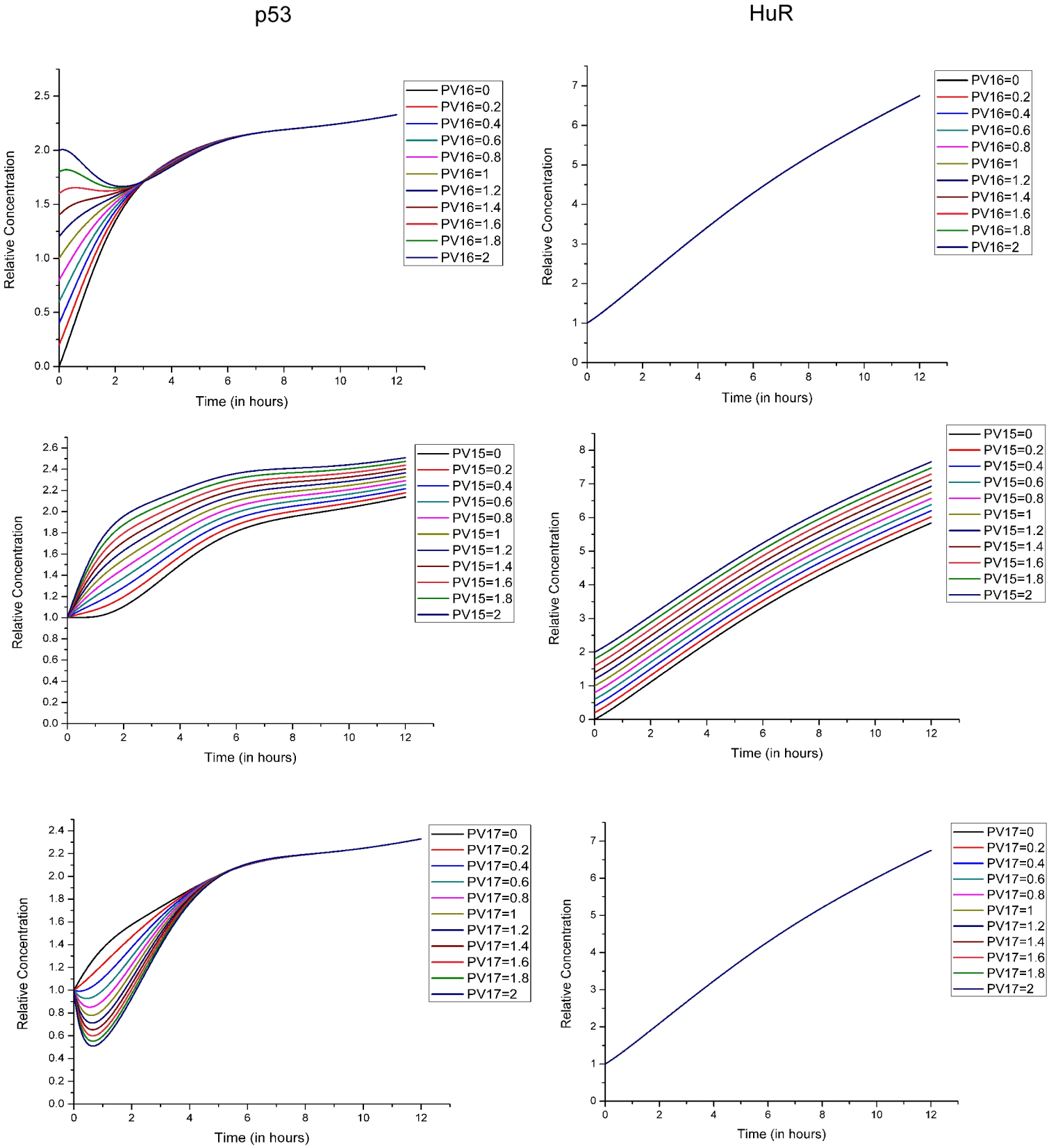

Estimation of robustness of Model 3 **(Figure 2E)** by varying assumed parameters (initial conditions: p53 concentration (PV16) = 1, HuR concentration (PV15) = 1, and Mdm2 concentration (PV17) = 0.05) between 0-2.

Figure S15. Related to Figure 3.

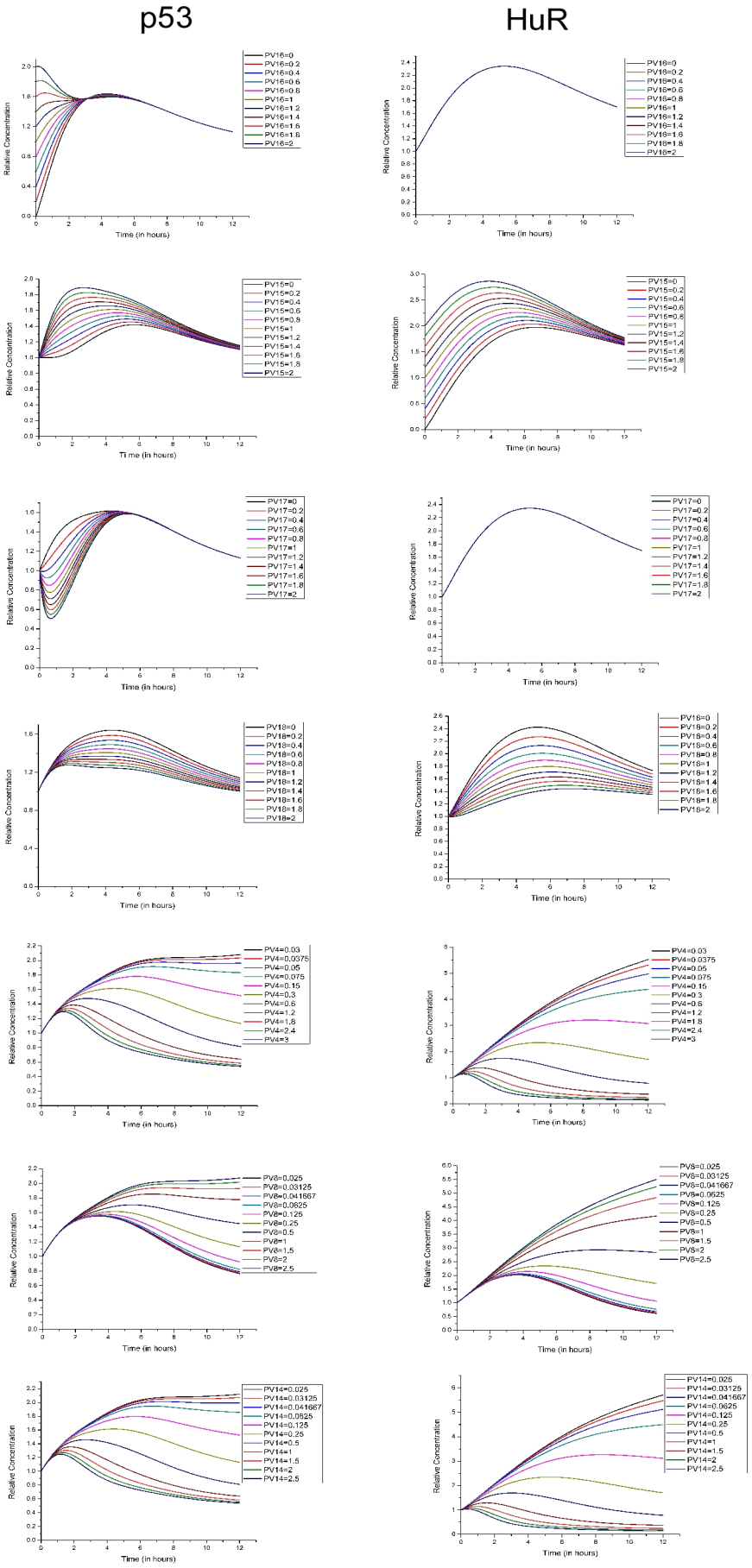

Estimation of robustness of Model 4 **(Figure 3D)** by varying of initial conditions (p53 concentration (PV16) = 1, HuR concentration (PV15) = 1, Mdm2 concentration (PV17) = 0.05 and X concentration (PV18) = 0.1) between 0-2 and assumed parameters (K_{XH}(PV14) = 0.5, α_X(PV4) = 0.2 and β_X(PV8) = 0.15) over a 10-fold range of values

Figure S16. Related to Figure 7.

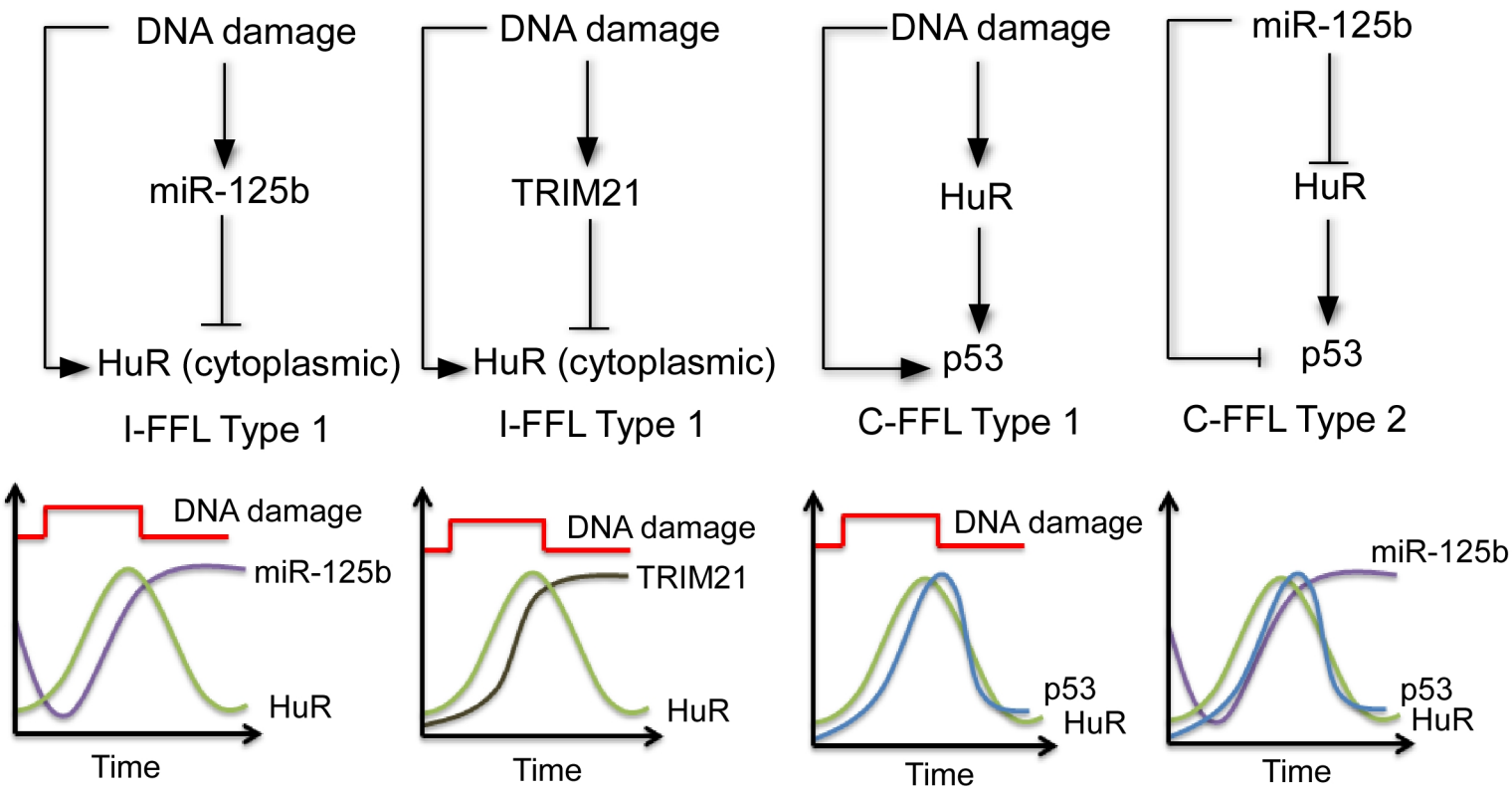

Schematic diagrams of the three Type 1 and one Type 2 incoherent and coherent feed forward loops in the translation regulatory network regulating p53 expression in response to UV-induced DNA damage. The outputs of the individual feed forward loops show expression patterns of HuR, p53, miR-125b and TRIM21 in response to DNA damage, taken as a step function.

Table S1. Related to Figures 1, 2, and 3

Model details: Parameters and initial conditions

PV	Parameter	Description	Values	Source
1	α_{HuR}	Cytoplasmic HuR accumulation rate	0.6	Experimental
2	α_{p53}	p53 synthesis rate	0.4	Experimental
3	α_{Mdm2}	Mdm2 synthesis rate	0.2	Literature[1]
4	α_{X}	X synthesis rate	0.3	Assumed
5	β_{HuR}	HuR degradation rate	0.008	Experimental
6	β_{p53}	p53 degradation rate	0.22	Experimental
7	β_{Mdm2}	Mdm2 degradation rate	1	Literature[1]
8	β_{X}	X degradation rate	0.25	Assumed
9	k_{mH}	miR-125b dependent HuR repression rate	0.309	Experimental
10	k_{mp}	miR-125b dependent p53 repression rate	0.271	Experimental
11	k_{Hp}	HuR dependent p53 production rate	1.185	Experimental
12	k_{pM}	p53 dependent mdm2 production rate	0.9	Literature[1]
13	k_{Mp}	Mdm2 dependent p53 degradation rate	1.4	Literature[1]
14	k_{XH}	X dependent HuR degradation rate	0.25	Assumed
15	HuR_0	Initial HuR concentration	1	Assumed
16	$p53_0$	Initial p53 concentration	0.55	Assumed†
17	$Mdm2_0$	Initial Mdm2 concentration	0.05	Assumed
18	X_0	Initial X concentration	0.1	Assumed

† For minimal model, initial concentration of p53 was taken as 0.55 for simulation and then scaling was done to 1 for initial concentration of p53 for plotting.

References

[1] Eric Batchelor, Caroline Mock, Irun Bhan, Alexander Loewer, and Galit Lahav. Recurrent Initiation: A Mechanism for Triggering p53 Pulses in Response to DNA Damage. Molecular Cell , Volume 30 , Issue 3 , 277 – 289.

Table S2. Related to Figure 4

Comparison of Proteins identified in LC-MS analysis.

Protein	accession	Mass Da	Spectral Counts		SC ratio
			IgG	HuR	HuR/Con
78 kDa glucose-regulated protein precursor	16507237	72402	20	0	0.00
actin, cytoplasmic 1	4501885	42052	13	0	0.00
ATP synthase subunit beta, mitochondrial precursor	32189394	56525	6	0	0.00
cold-inducible RNA-binding protein	4502847	18637	6	0	0.00
DNA damage-binding protein 1	148529014	128142	35	0	0.00
fructose-bisphosphate aldolase A isoform 1	4557305	39851	3	0	0.00
hemoglobin subunit alpha	4504345	15305	7	0	0.00
lanC-like protein 1	5174445	45995	19	0	0.00
PREDICTED: probable ATP-dependent RNA helicase DDX46 isoform X1	530380277	117902	11	0	0.00
serine/arginine-rich splicing factor 2	47271443	25461	5	0	0.00
S-phase kinase-associated protein 1 isoform a	25777711	18223	8	0	0.00
splicing factor U2AF 65 kDa subunit isoform a	6005926	53809	10	0	0.00
stress-70 protein, mitochondrial precursor	24234688	73920	27	1	0.04
putative RNA-binding protein Luc7-like 2 isoform 1	116812577	46942	18	1	0.06
serine/arginine-rich splicing factor 1 isoform 1	5902076	27842	18	1	0.06
tubulin beta chain	29788785	50095	52	6	0.12
splicing factor U2AF 35 kDa subunit isoform a	5803207	28368	8	1	0.13
ATP synthase subunit alpha, mitochondrial isoform a precursor	4757810	59828	7	1	0.14
serine/arginine-rich splicing factor 3	4506901	19546	12	2	0.17
tubulin alpha-1B chain	57013276	50804	27	5	0.19
40S ribosomal protein S5	13904870	23033	5	1	0.20
annexin A2 isoform 2	4757756	38808	5	1	0.20
galectin-7	4504985	15123	4	1	0.25
protein-L-isoaspartate(D-aspartate) O-methyltransferase isoform 1	226530908	30524	8	2	0.25
serum albumin preproprotein	4502027	71317	20	5	0.25
protein S100-A8	21614544	10885	7	2	0.29
alpha-enolase isoform 1	4503571	47481	34	10	0.29
signal recognition particle 14 kDa protein	149999611	14675	3	1	0.33
protein S100-A9	4506773	13291	16	6	0.38
RNA-binding protein FUS isoform 1	4826734	53622	16	6	0.38
RNA-binding motif protein, X chromosome isoform 1	56699409	42306	13	5	0.38

glyceraldehyde-3-phosphate dehydrogenase isoform 1	7669492	36201	33	13	0.39
activated RNA polymerase II transcriptional coactivator p15	217330646	14386	10	4	0.40
desmocollin-1 isoform Dsc1b preproprotein	4826702	94916	10	4	0.40
RNA-binding protein EWS isoform 2	4885225	68721	5	2	0.40
heat shock 70 kDa protein 1A/1B	167466173	70294	107	43	0.40
protein S100-A7	115298657	11578	19	8	0.42
peroxiredoxin-1	4505591	22324	16	7	0.44
desmoplakin isoform I	58530840	334021	34	15	0.44
elongation factor 1-alpha 1	4503471	50451	13	6	0.46
40S ribosomal protein S19	4506695	16051	16	8	0.50
60S ribosomal protein L37a	4506643	10497	4	2	0.50
nucleolin	55956788	76625	4	2	0.50
desmoglein-1 preproprotein	119703744	114702	22	12	0.55
small nuclear ribonucleoprotein Sm D3	4759160	14021	9	5	0.56
macrophage migration inhibitory factor	4505185	12639	7	4	0.57
heterogeneous nuclear ribonucleoprotein U isoform b	14141161	89665	5	3	0.60
60S ribosomal protein L23a	17105394	17684	8	5	0.63
60S ribosomal protein L12	4506597	17979	17	11	0.65
60S ribosomal protein L21	18104948	18610	6	4	0.67
prolactin-inducible protein precursor	4505821	16847	7	5	0.71
dermcidin preproprotein	16751921	11391	11	8	0.73
junction plakoglobin	4504811	82434	6	5	0.83
THO complex subunit 4	238776833	27541	29	25	0.86
40S ribosomal protein S12	14277700	14905	6	6	1.00
malate dehydrogenase, mitochondrial isoform 1 precursor	21735621	35937	3	3	1.00
small nuclear ribonucleoprotein Sm D1	5902102	13273	6	6	1.00
high mobility group protein B1	4504425	25049	9	10	1.11
40S ribosomal protein S25	4506707	13791	7	8	1.14
60S ribosomal protein L23	4506605	14970	12	14	1.17
60S ribosomal protein L38	4506645	8270	8	11	1.38
60S acidic ribosomal protein P2	4506671	11658	21	30	1.43
60S acidic ribosomal protein P1 isoform 1	4506669	11621	6	10	1.67
histone H2B type 1-C/E/F/G/I	4504257	13898	4	8	2.00
ELAV-like protein 1	38201714	36240	0	6	HuR only

serpin B3	5902072	44565	0	2	HuR only
E3 ubiquitin-protein ligase TRIM21	15208660	54170	0	4	HuR only

Transparent Methods

Modelling procedure

Rate equations representing the rate of change of concentration of network components over time were represented by non-linear differential equations consisting of synthesis and degradation terms and regulatory terms representing the effect of other network components. Complete model details, initial conditions and parameters are provided in **Table S1**. The set of differential equations for each model were numerically integrated with the parametric values which were either obtained experimentally, or from literature or assumed. Differential equations were solved by ODE45 module MATLAB (Version R2010b. MathWorks). Curve fitting was done using Curve Fitting Toolbox.

Plasmid constructs

The 1208 nt HuR mRNA 3'UTR containing the putative miR-125b target site (nt 671-693) was isolated from human leukocyte RNA by RT-PCR and cloned downstream of firefly luciferase gene in pCDNA3-Fluc vector. The miR-125b target site was mutated using site directed mutagenesis and cloned into the same vector. The double-stranded DNA oligo encoding miR-125b was cloned into pSUPER vector (Oligoengine) containing the EGFP gene to produce shRNA corresponding to miR-125b. HuR cDNA cloned with a myc-tag in pCDNA3.1 vector and TRIM21 expression construct (gift from Sunit. K. Singh, BHU, Varanasi, India) were used for mammalian expression of HuR and TRIM21 respectively. Expression construct for Haemagluttinin (HA)-tagged ubiquitin was a kind gift from S.N. Bhattacharyya, CSIR-IICB, Kolkata, India.

Cell culture, treatment and transfection

MCF7 and MDA-MB-231 human breast carcinoma cells were maintained in Dulbecco's modified Eagle's Medium (Thermo Fisher Scientific) with 10% FBS and 1% Pen-Strep. Cells were exposed to a 10 J/m^2 pulse of short wavelength UV (UVC) irradiation in UVC crosslinker. Cells were treated with 100 μg/ml cycloheximide (Amresco) or 5 μM MG132 (Sigma Aldrich). Cells were transfected with different vectors, siRNAs (siGENOME SMART pool, TRIM21) and Non Targeting siRNA pool (Dharmacon) and antagomiR against miR-125b (Trilink Biotechnologies) using Lipofectamine 2000 (Thermo Fisher Scientific) in DMEM low glucose medium (Thermo Fisher Scientific). DNA amount for transfection with plasmid constructs was equalised by pGEMT plasmid (Promega).

Reporter assay

Cells transfected with firefly luciferase HuR 3'UTR reporter gene constructs and a Renilla luciferase construct were lysed with passive lysis buffer 48 hours post transfection. Luciferase assay was performed using Dual-Glo Luciferase assay system (Promega) following manufacturer's protocol. Luminescence was measured in a Plate Chameleon V (Hidex) multilabel microplate reader.

Immunoblotting

Cells were lysed in S10 lysis buffer (10 mM HEPES, 15 mM KCl, 1 mM PMSF, 1 mM DTT, 0.1% Triton X100) and centrifuged at 10,000 x g for 20 minutes for cytoplasmic lysate preparation. Lysates were quantified using Bradford reagent (Amresco), resolved on 12% SDS-PAGE and were immunoblotted using anti HuR (3A2, Santa Cruz Biotechnology), p53 (DO-1, Santa Cruz Biotechnology), TRIM21 (E-11, Santa Cruz Biotechnology), Ubiquitin (P4D1, Cell

Signaling Technologies), Myc (71D10, Cell Signaling Technologies), HA (6E2, Cell Signaling Technologies) β-actin (A00730, Genscript) and GAPDH (FL-335, Santa Cruz Biotechnology) antibodies. Chemiluminescent signal was detected using Femtolucent Plus HRP (Geno Biosciences).

RNA Immunoprecipitation

A 50% slurry of pre-swelled Protein A Sepharose beads (Sigma Aldrich) was incubated with specific antibodies overnight at 4˚C. 500 µg of pre-cleared lysate was added to the bead-antibody mix and incubated for 4hrs at 4°C and washed five times with NT2 (50 mM Tris Chloride (pH7.4), 150 mM NaCl, 1 mM $MgCl_2$, 0.05% NP-40) buffer. RNA was isolated from the immunoprecipitated complexes by Trizol (Thermo Fisher Scientific) followed by qPCR with HuR 3'UTR specific primers and GAPDH primers as control.

Coimmunoprecipitation

Cells treated with UV and MG132 were lysed with Pierce Direct IP kit IP lysis buffer (Thermo Fisher Scientific). Lysates were immunoprecipitated with anti-HuR, anti-TRIM21 or anti-HA antibody using Pierce Direct IP kit using manufacturer's protocol. The bound antigen was eluted with elution buffer and immunoblotting was performed with specific antibodies to detect co-immunoprecipitated proteins.

Quantitative PCR

Total cellular RNA was extracted using Trizol and polyadenylated using Poly A polymerase (New England Biolabs). cDNA was synthesised using oligo(dT)-adapter primer by MuMLV reverse transcriptase (Thermo Fisher). An adapter-specific primer and microRNA-125b specific primer (miScript primer assay kit, Qiagen) with Power SYBR Green master mix (Applied

Biosystems) were used for qPCR reactions in Step One Plus Real time PCR system (Applied Biosystems). 3'UTR-specific primers were used for detection of HuR mRNA. Firefly luciferase specific primers were used for detection of Firefly luciferase mRNA having HuR 3'UTR. U6B snRNA (miScript primer assay kit, Qiagen) and GAPDH primers were used for miRNA and mRNA quantity normalisation respectively.

Polysome analysis

Transfected cells were treated with Cycloheximide (100ug/ml) for 30 minutes and lysed with polysome lysis buffer (20 mM Tris-chloride (pH 7.4), 5 mM $MgCl_2$, 150 mM NaCl, 1 mM DTT, 0.2 mM PMSF, 0.5% NP40, 1X protease inhibitor, 100 U/ml RNase Inhibitor) containing cycloheximide. Cytosolic extract was obtained by centrifugation at 10,000 x g for 20 min. 50 OD (260 nm) of cell lysate was loaded on 10-50% (w/v) sucrose gradient followed by centrifugation at 100,000 x g, at 4˚C for 4 hours. Fractions were collected using a programmable gradient fractionator (Biocomp Instruments) and absorbance of fractions was measured at 254nm. RNA was isolated from the fractions by phenol-chloroform extraction and ethanol precipitation and subsequently used for RT-PCR using gene-specific primers.

Mass spectrometry

Cells overexpressing HuR were exposed to UV irradiation and treated with MG132 were lysed 6 hours after UV exposure and lysates were immunoprecipitated with anti-HuR antibody and IgG. The IP eluates were diluted with 6M urea, 100 mM Tris pH 8.0. Trypsin digestion was carried out by adding approximately 10 µl of 0.1 µg/µl trypsin in 100 mM Tris and incubating overnight at room temperature. LC-MS/MS was performed on a Finnigan LTQ-Obitrap Elite hybrid mass spectrometer system (Thermo Fisher Scientific). The data were analyzed by using all CID

spectra collected in the experiment to search the human reference sequence database with the search program Mascot. The total number of spectra, termed spectral counts, was compared for proteins in the IP and control samples.

Ubiquitination assay

Cells treated with UV and MG132 and/or transfected with siRNAs or cotransfected with HA-ubiquitin and Myc-tagged HuR constructs were lysed and lysates (supplemented with 0.5mM ATP) were immunoprecipitated with anti-HuR antibody or anti-HA antibody. Immunoprecipitates were resolved on SDS-10%PAGE and immunoblotted with anti-Ubiquitin antibody or anti-Myc antibody.

Cell viability assay

24 hours post transfection with control oligo, antagomiR-125b, TRIM21 siRNA or both, 10^4 cells were UV irradiated and cell viability was determined at designated time points using MTT assay reagent (Sigma Aldrich).

Statistical analysis

All graphical data represent mean ± standard deviation of at least three independent experiments (biological replicates). The fit of simulated plots to experimentally obtained plots was tested by Pearson's R test. * or # signifies a p-value ≤ 0.05, ** or ## signifies a p-value ≤ 0.01, *** or ### signifies a p-value ≤ 0.005 (Paired two-tailed or one-tailed Students t test as applicable) between controls and samples indicated in the Figures.